Neutralizing antibodies impair the oncolytic efficacy of reovirus but permit effective combination with T cell-based immunotherapies

Groeneveldt, C.; Kinderman, P.; Griffioen, L.; Rensing, O.; Labrie, C.; Wollenberg, D.J.M. van den; ... ; Montfoort, N. van

Neutralizing Antibodies Impair the Oncolytic Efficacy of Reovirus but Permit Effective Combination with T cell–Based Immunotherapies

Christianne Groeneveldt[1], Priscilla Kinderman[2], Lisa Griffioen[1], Olivia Rensing[2], Camilla Labrie[1], Diana J.M. van den Wollenberg[3], Rob C. Hoeben[3], Matt Coffey[4], Houra Loghmani[4], Els M.E. Verdegaal[1], Marij J.P. Welters[1], Sjoerd H. van der Burg[1], Thorbald van Hall[1], and Nadine van Montfoort[2]

ABSTRACT

Reovirus type 3 Dearing (Reo), manufactured for clinical application as pelareorep, is an attractive anticancer agent under evaluation in multiple phase 2 clinical trials for the treatment of solid tumors. It elicits its anticancer efficacy by inducing both oncolysis and intratumoral T-cell influx. Because most people have been preexposed to Reo, neutralizing antibodies (NAb) are prevalent in patients with cancer and might present a barrier to effective Reo therapy. Here, we tested serum of patients with cancer and healthy controls ($n = 100$) and confirmed that Reo NAbs are present in >80% of individuals. To investigate the effect of NAbs on both the oncolytic and the immunostimulatory efficacy of Reo, we established an experimental mouse model with Reo preexposure. The presence of preexposure-induced NAbs reduced Reo tumor infection and prevented Reo-mediated control of tumor growth after intratumoral Reo administration. In B cell–deficient mice, the lack of NAbs provided enhanced tumor growth control after Reo monotherapy, indicating that NAbs limit the oncolytic capacity of Reo. In immunocompetent mice, intratumoral T-cell influx was not affected by the presence of preexposure-induced NAbs and consequently, combinatorial immunotherapy strategies comprising Reo and T-cell engagers or checkpoint inhibitors remained effective in these settings, also after a clinically applied regimen of multiple intravenous pelareorep administrations. Altogether, our data indicate that NAbs hamper the oncolytic efficacy of Reo, but not its immunotherapeutic capacity. Given the high prevalence of seropositivity for Reo in patients with cancer, our data strongly advocate for the application of Reo as part of T cell–based immunotherapeutic strategies.

Introduction

Oncolytic viruses (OV) represent a highly promising treatment strategy for a wide range of cancers. They mediate both the direct killing of tumor cells and the induction of potent immune responses. The immunostimulatory properties of OVs can be exploited to convert the cold tumor microenvironment (TME) of solid tumors into a T cell–infiltrated TME, leading to an increased response to other forms of immunotherapy (1). Oncolytic reovirus type 3 Dearing (Reo) is one of the leading OVs for clinical development (2). In our previous studies using the preclinical murine pancreatic KPC3 tumor model, Reo induced a strong IFN response in these tumors, which subsequently attracted a wave of $CD8^+$ T cells. These immunostimulatory characteristics enabled Reo to significantly enhance the efficacy of otherwise unsuccessful CD3xTRP1-bispecific antibody therapy in these tumors (3).

In the clinic, Reo has demonstrated limited potential when applied as monotherapy (4–6). Although various aspects might contribute to this limited efficacy, one potential barrier to the clinical success of Reo is preexisting immunity against the virus (7). The majority of individuals acquire preexisting immunity against reovirus after nonsymptomatic exposure, and this is indicated by the detection of neutralizing antibodies (NAb) in patient sera before treatment with Reo (5, 8–12). It has been demonstrated that Reo can still reach the TME in the presence of NAbs, as it can be carried there via circulating immune cells (13). Because additional studies demonstrated that the uptake and delivery of Reo particles to the tumor via these cellular carriers is enhanced in the presence of NAbs (14, 15), this led to a common belief that NAbs do not represent a barrier and may even be beneficial for reovirus therapy. But, to the best of our knowledge, a direct comparison of the antitumor efficacy of Reo therapy in settings with and without preexisting NAbs has not been performed.

To address this knowledge gap, we developed an experimental setting in immunocompetent mice to study the effect of preexposure- or therapy-induced NAbs on both the oncolytic and the immunostimulatory capacity of Reo. We found that NAbs hampered Reo infection and the Reo-induced expression of IFN-stimulated genes (ISG) and prevented Reo-mediated control of tumor growth. However, NAbs did not impair the Reo-induced intratumoral T-cell influx, and T cell–based viro-immunotherapeutic combination strategies remained effective, even in the context of clinically preferred intravenous administration. Thus, this study demonstrates that preexisting immunity is detrimental to Reo monotherapy, but that Reo can still be used to sustain effective T cell–based immunotherapy.

Materials and Methods

Virus

The wild-type reovirus strain R124 (herein referred to as Reo) was previously isolated from a heterogeneous Reo (T3D; stock VR-824,

[1]Department of Medical Oncology, Oncode Institute, Leiden University Medical Center, Leiden, the Netherlands. [2]Department of Gastroenterology and Hepatology, Leiden University Medical Center, Leiden, the Netherlands. [3]Department of Cell and Chemical Biology, Leiden University Medical Center, Leiden, the Netherlands. [4]Oncolytics Biotech Incorporated, Calgary, Canada.

Corresponding Author: Nadine van Montfoort, Leiden University Medical Center, C4-P, Albinusdreef 2, 2333 ZA, Leiden, the Netherlands. E-mail: nvanmontfoort@lumc.nl

Cancer Immunol Res 2024;12:334–49

doi: 10.1158/2326-6066.CIR-23-0480

obtained from the ATCC) by two rounds of plaque purification using HER911 cells (16). All experiments were performed using cesium chloride-purified stocks prepared as previously described (3). The total number of particles was calculated on the basis of OD_{260} values, where 1 OD equals 2.10×10^{12} reovirus particles/mL (17), and the infectious titer was quantified by plaque assay on HER911 cells as previously described (18). Clinical-grade Reo (pelareorep) was provided by Oncolytics Biotech Incorporated (Calgary, AB, Canada). Vesicular stomatitis virus (VSV)ΔM51-GFP is a recombinant derivative of the VSV Indiana serotype (19) engineered to carry a GFP reporter gene as previously described (20); it was provided by John Hiscott and Michela Muscolini (Istituto Pasteur Italia-Fondazione Cenci Bolognetti, Rome, Italy).

Serum from healthy volunteers and patients with cancer

Serum samples from the various cancer patient cohorts were obtained during various Phase I/II studies that were approved by the Medical Ethics Committee of the Leiden University Medical Center (LUMC) and conducted in accordance with the Declaration of Helsinki. All patients gave written informed consent before inclusion in the respective studies. The use of serum samples and corresponding geographical data (gender, age) from these cohorts for this study was approved by the LUMC Biobank Review Committee under reference number RP23.023. Serum from healthy donors ($n = 25$) was obtained through the Leiden University Medical Center (LUMC) Voluntary Donor Service (LuVDS, Leiden, the Netherlands) after ethical approval under reference number LuVDS22.049. The age of healthy donors was matched to the age range within the cancer patient cohorts.

The various Phase I/II studies from which samples were used are as follows. Patients with recurrent Epithelial Ovarian Cancer from the "Ovarium Carcinoma" cohort (study number NCT01637532; $n = 21$) were treated to evaluate the safety and feasibility of tocilizumab in combination with carboplatin/(pegylated liposomal) doxorubicin and IFNα2b (Peg-Intron; ref. 21). Patients in the "Melanoma" cohort (study number P04.085; $n = 15$) were treated with adoptive T-cell transfer consisting of tumor-reactive autologous T cells (22). Patients from the "Cervical Carcinoma" cohort ($n = 19$) were included in the CIRCLE study investigating cellular immunity against anogenital lesions (23). Patients with metastatic colorectal cancer from the "Colon Carcinoma" cohort (study number ISRCTN43704292; $n = 20$) were enrolled in a phase I/II trial investigating the safety and efficacy of a p53-synthetic long peptide vaccine (24). Serum samples were collected during the respective clinical studies and stored at −80°C until use.

Cell lines and culture

The murine pancreatic cancer cell line KPC3 (RRID:CVCL_A9ZK) is a low-passage derivate of a primary KPC tumor with mutant *Trp53* and *K-ras* from a female C57BL/6 mouse (3, 25). KPC3.TRP1 cells (RRID:CVCL_A9ZL) were generated as previously described (26) and selected for expression of tyrosine-related protein (TRP1) by cell sorting using a TRP1-specific antibody (clone: TA99, Santa Cruz Biotechnology, #sc-58438). The MC38 cell line (RRID: CVCL_B288) is a chemically induced murine colon carcinoma and was obtained from Prof. F. Ossendorp (Leiden University Medical Center, the Netherlands). The human breast cancer cell line BT474 (RRID: CVCL_0179) was purchased from the ATCC (ATCC-HTB-20). KPC3(.TRP1), MC38, and BT474 cells were cultured at 37°C in a humidified atmosphere containing 5% CO_2 in IMDM (Gibco, #12440053) supplemented with 8% FCS (Bodinco, Alkmaar, the Netherlands, #5010), 2 mmol/L L-glutamine (Gibco, #25030081), 100 U/mL penicillin and 100 μg/mL streptomycin (Gibco, #15140122). The human embryonic retinoblast cell line HER911 (RRID:CVCL_1K15) was cultured in DMEM (Gibco, #11965092), supplemented as described above. The tumor cell line TC1 (RRID: CVCL_4699) expresses the HPV16-derived oncogenes E6 and E7 and activated Ras oncogene and was cultured in IMDM medium as described above but with the addition of 400 μg/mL Geneticin (G418; Life Technologies, #10131027), 1% nonessential amino acids (Life Technologies, #11140050), and 1 mmol/L sodium pyruvate (Life Technologies, #11360070; ref. 27). Cell lines were assured to be free of *Mycoplasma* by regular PCR analysis. The authentication of the cell lines was done by Short Tandem Repeat (STR) profiling (IDEXX BioAnalytics, Ludwigsburg, Germany) and only cells with passage number <7 were used for experiments.

Antibodies and reagents for *in vivo* administration

The CD3xTRP1 bispecific antibody (bsAb; Absolute Antibody, bAb0136) we used is a knob-into-hole bispecific based on murine IgG2a with an Fc Silent mutation, featuring one arm with an anti-mouse CD3e scFv based on the clone 145–2C11, and the other arm containing the TA99 clone directed against TRP1. PD-L1 blockade was performed using a PD-L1–blocking antibody (clone 10F.9G2; GoIn-Vivo Purified anti-mouse CD274 Antibody; BioLegend). The CD20-specific antibody (clone 18B12) was obtained from Absolute Antibody, and CD8-specific (clone 2.43), CD4-specific (clone GK1.5) and NK1.1-specific (clone PK136) antibodies were all obtained from BioXcell. Clodronate liposomes were obtained from Liposoma BV (Amsterdam, the Netherlands).

Animal experiments

Male C57BL/6J mice (RRID:IMSR_JAX:000664; 6–8-weeks-old) were purchased from Charles River Laboratories. Male B6.129S2-Ighm^{tm1Cgn}/J mice (μMT; RRID:IMSR_JAX:002288; 6–8-weeks-old) were purchased from The Jackson Laboratory. Male and female nonobese diabetic (NOD).Cg-Prkdc^{scid}Il2rg^{tm1Wjl}/SzJ (NSG) mice (RRID:IMSR_JAX:005557; 6–16-weeks-old) were obtained from The Jackson Laboratory and maintained at the breeding facility of the LUMC in Leiden, the Netherlands.

All mouse experiments were individually prepared, reviewed, ethically approved, and registered by the institutional Animal Welfare Body of the LUMC and carried out under project license AVD1160020187004, issued by the competent authority on animal experiments in the Netherlands (named CCD). Experiments were performed following the Dutch Act on Animal Experimentation and EU Directive 2010/63/EU ("On the protection of animals used for scientific purposes") at the animal facility of the LUMC. Mice were housed in individually ventilated cages with no more than 5 mice/cage and experiments were initiated after one week of acclimatization after transport.

For preexposure, mice were injected intravenously with 10^7 plaque-forming units (pfu) of Reo or VSV in a volume of 100 μL PBS (Fresenius Kabi) at two consecutive times with a 2-week interval. This preexposure dose resulted in NAb levels and corresponding IC_{50} values (see section "*Neutralization assay to measure NAb levels*" for the method used to calculate IC_{50} values) that were comparable with IC_{50} values in highly seropositive human individuals. In depletion experiments, depletion using CD20-specific, NK1.1-specific, CD8-specific, or CD4-specific antibodies (100 μg in 100 μL PBS, intraperitoneally) was initiated 5 and 2 days before the first Reo preexposure, and thereafter depletion was maintained by weekly injections until indicated. Alternatively, anti-CD4 injections were initiated before the second Reo preexposure or before tumor challenge. Clodronate

liposomes (1.5 mg, i.p.) were administered every 5 days, starting 7 days before the first Reo preexposure. Depletion of designated cell populations was verified by flow cytometry before mice received further interventions. The administration of clodronate liposomes at the manufacturer's recommended dose impaired the wellbeing of the mice and caused significant weight loss in some of the mice (Supplementary Fig. S1), which forced us to terminate the experiment to prevent more severe discomfort. We were therefore unable to assess the effect of clodronate liposome treatment on the intratumoral influx of Reo-specific $CD8^+$ T cells.

After preexposure or at the start of the experiment, mice were inoculated in the right flank with subcutaneous KPC3(.TRP1) tumors (1×10^5 cells in 100 μL PBS/0.1% BSA; Sigma-Aldrich, #A3912) or MC38 tumors (5×10^5 cells in 200 μL PBS/0.1% BSA). BT474 tumors were orthotopically engrafted by injecting a total of 5×10^6 cells in a volume of 100 μL 1:1 (v/v) PBS/0.1% BSA:Growth Factor Reduced Matrigel (Corning, #356231) in the fourth mammary fat pad of isoflurane-anesthetized female NSG mice. Mice with palpable tumors were allocated into groups with similar average tumor volumes and assigned a treatment regimen. Intratumoral Reo or VSV administration was performed under isoflurane anesthesia by injection of 10^7 pfu of Reo or VSV or PBS as a control in a volume of 30 μL on 3 consecutive days unless otherwise indicated. Intravenous pelareorep administration was performed by injection of a total of 2×10^8 pfu of pelareorep in a volume of 100 μL PBS in the tail vein on indicated days, with 5-day intervals. Treatment with CD3xTRP1 bsAbs consisted of 3 intraperitoneal injections of 12.5 μg antibody in 100 μL PBS, given every other day or with 5-day intervals. PD-L1–specific antibodies were administered on indicated days by intraperitoneal injection of 200 μg antibody in 100 μL PBS.

Cages were randomly allocated to a certain treatment group by an independent researcher and treatments were given in a different order each time. During all experiments, tumor volume and/or body weight were measured 3 times a week in 3 dimensions using a caliper, in a blinded manner concerning preexposure status, genotype, or depletion group when possible. Tumor volume was calculated by multiplying length x width x height. Blood was collected in lithium heparin-coated microvettes (Sarstedt) from the tail vein on indicated days for interim analysis of immune cells. Plasma was obtained by centrifugation of blood (14,000 rpm, 15 minutes, 4°C) and stored at −80°C for assessment of NAbs.

For tumor growth experiments, mice were sacrificed when the tumor volume exceeded 1,000 mm^3 or when ulceration occurred. Therapy response was determined as follows: no response (NR); complete response (CR); and partial response (PR; regression or constant tumor volumes for at least 7 days). For intratumoral analysis experiments, mice were sacrificed at indicated days after treatment, and tumors, spleens, tumor-draining lymph nodes (TDLN), and blood were collected. Tumors were divided into representative parts, which were either snap-frozen in liquid N_2 and stored at −80°C until further analysis, fixed in 4% formaldehyde (AddedPharma) for IHC or immediately processed to single-cell suspensions to analyze the cellular composition by flow cytometry.

Neutralization assay to measure NAb levels

HER911 cells were seeded in flat-bottom 96-well plates at a density of a total of 1×10^4 cells/well and allowed to adhere overnight in the incubator (37°C, 5% CO_2, 90% humidity). The next day, human serum samples or murine plasma samples were heat-inactivated by incubation at 56°C for 30 minutes. For human serum samples, a 2-fold dilution series (starting with 1:5) was prepared in duplicate in DMEM with 2% FCS (Bodinco, #5010). Nanogam (Sanquin, Amsterdam, the Netherlands), which is a pool of immunoglobulins of >1,000 donors, was used as a positive control. For murine plasma samples, a 2- or 4-fold dilution series was prepared (starting with 1:25, 1:50, or 1:100) in DMEM with 2% FCS. Serum or plasma samples were mixed with 150 pfu/well of Reo or with 15 pfu/well of VSV and incubated for 30 minutes at 37°C to allow the binding of NAbs to viral particles. Next, the serum/plasma:Virus complexes were transferred in duplicate onto the HER911 cells. Cell growth was determined at 3 days postinfection by crystal violet staining. Briefly, cells were fixed with ice-cold methanol (Merck) for 10 minutes at −20°C. Thereafter, cells were incubated with 0.5% crystal violet (Sigma-Aldrich, #C0775) in 20% methanol for 20 minutes at room temperature (RT). Plates were extensively washed with H_2O and air dried. After drying, plates were incubated with 100 μL of methanol for 20 minutes at RT before measuring the optical density (OD) at 570 nm using a SpectraMax iD3 multi-mode plate reader (Molecular Devices). The measured OD_{570} value of the positive control (virus only) was set to 0% cell growth and that of the negative control (medium only) to 100% cell growth. The OD_{570} of the samples were normalized using these controls and IC_{50} values were calculated using nonlinear regression analysis and sera with $IC_{50} < 10$ were regarded as negative.

Cell preparation and flow cytometry

Tumors were minced in small pieces and incubated with Liberase TL (Roche, #05401020001) for 15 minutes at 37°C. The reaction was stopped by the addition of culture medium with 8% FCS and the mixture was gently dissociated into a single-cell suspension over a cell strainer (Corning). Spleens and TDLNs were dissociated into a single-cell suspension over a cell strainer. Blood and splenocytes were incubated with lysis buffer (Pharmacy LUMC) for 3 minutes at RT to remove all red blood cells before use. Cells were incubated with Zombie Aqua Fixable Viability Dye (BioLegend, #423102) in PBS for 20 minutes at RT followed by incubation with 2.4G2 FcR blocking antibodies (clone 2.4G2; BD Biosciences, #553142) in FACS buffer (PBS, 0.5% BSA, and 1% sodium azide) for 20 minutes on ice.

If applicable, cells were incubated with Reo $\mu1_{133-140}$ tetramer (Tm) conjugated to APC, the Reo $\mu1_{422-430}$ Tm conjugated to PE or the VSV NP_{52-59} Tm conjugated to APC. These tetramers were generated *in-house* by the peptide and MHC-tetramer facility of the LUMC, according to the protocol described in (28) with H2-K^b or H2-D^b instead of MHC-E. Samples were incubated with the tetramers for 1 hour at RT in FACS buffer, after which antibodies specific for surface markers (Supplementary Table S1) were added directly to the tetramer mixture and incubated for 30 minutes at RT. After completion of the staining protocol (see Supplementary Fig. S2 for the gating strategy), samples were fixed in 1% paraformaldehyde (Pharmacy LUMC) and acquired using a BD LSRFortessa X20 4 L cell analyzer (BD Biosciences) at the Flow cytometry Core Facility (FCF) of the LUMC (https://www.lumc.nl/en/research/facilities/flow-cytometry-core-facility/). Data were analyzed using FlowJo Software Version 10 (Becton, Dickinson, and Company). Opt-SNE plots (29) were generated using standard settings in OMIQ data analysis software (Omiq, Inc. www.omiq.ai).

Intracellular cytokine staining

Ex vivo tumor single-cell suspensions were cocultured with Reo-infected TC1 cells [multiplicity of infection (MOI) = 10] or Reo-derived peptides (1 μg/mL) to assess recognition. Sequences of Reo-derived peptides (Supplementary Table S2) were obtained from a

study by Murphy and colleagues (30) in which the MHC-I ligandome of Reo-infected ovarian surface epithelial cells (ID8; H2-K^b/H2-D^b) was investigated using comparative mass spectrometry. Identified Reo-derived peptides were ordered as a micro-scale crude peptide library (GenScript). Effector cells (tumor single-cell suspensions) and target cells (Reo-infected TC1 cells) or peptides were cocultured for 6 hours in the presence of BD GolgiPlug (BD Biosciences, #555029/51–2301KZ). PMA (20 ng/mL; Sigma-Aldrich, #P8139) and ionomycin (1 μg/mL; Invitrogen, #I24222) were used as a positive control. After incubation, cells were washed and stained for CD8 (clone 53–6.7; BioLegend). Thereafter, cells were fixed with Fixation Buffer (BioLegend, #421002) according to the manufacturer's instructions, followed by staining for intracellular IFNγ (clone XMG1.2; BioLegend) in Permeabilization Wash Buffer (BioLegend #421002). After completion of the staining protocol, samples were fixed in 1% paraformaldehyde and acquired using the BD LSRFortessa X20 4 L cell analyzer.

Western blotting

The presence of antibodies against Reo proteins in the plasma of naive or preexposed mice was investigated by Western blotting. HER911 cells were infected with reovirus (MOI = 10) for 24 hours, after which cells were lysed in radioimmunoprecipitation assay buffer (Bioke, #9806S) containing protease inhibitors (Thermo Fisher Scientific, #78430) and phosphatase inhibitors (Thermo Fisher Scientific, #78428). Proteins (10–15 μg) were separated on a 4% to 15% mini-protean TGX gel (Bio-Rad, #4561086EDU) and then transferred to a 0.2 μmol/L nitrocellulose membrane (Bio-Rad). After blocking for 1 hour at RT with Pierce Protein-Free Blocking Buffer (Thermo Fisher Scientific, #37584), the membrane was incubated overnight at 4°C with pooled plasma from preexposed or naive mice (n = 5–6; 1:200). As a positive control, the membrane was incubated with anti-μ1 (clone 10F6; Developmental Studies Hybridoma Bank, 1:200). The next day, membranes were incubated with horseradish peroxidase (HRP)–conjugated goat anti-mouse IgG+IgM+IgA (1:1,000; Abcam, ab102445) at RT for 1 hour. Proteins were detected on the Chemidoc imaging XRS+ system (Bio-Rad) using the Clarity Western ECL Substrate kit (Bio-Rad, #1705061).

RNA isolation and qRT-PCR

Reo genomic copies and expression levels of host genes (see Supplementary Table S3 for primer sequences) in tumors were measured by qRT-PCR as previously described (3). Briefly, a representative snap-frozen proportion (10–30 mg) of each tumor or organ was disrupted in lysis buffer (Promega, #Z6112) using a stainless bead and the TissueLyser LT (Qiagen). Total RNA of tumor samples was isolated using the ReliaPrep RNA Tissue Miniprep System (Promega, #Z6112) according to the manufacturer's protocol. 500 ng of RNA was used to generate cDNA using the High-Capacity cDNA Reverse Transcription Kit (Thermo Fisher Scientific, #4368814) according to the manufacturer's protocol. Subsequent qPCR analysis was performed using the Bio-Rad iQ SYBR Green Supermix (Bio-Rad, #1708886) on a CFX384 Real-Time System machine (Bio-Rad). Reo S4 copy numbers were determined on the basis of a standard curve, generated with serial dilutions of plasmid pcDNA_S4. Log_{10} S4 copy numbers were calculated using a previously described formula (31). The expression of host genes was normalized to reference genes *Mzt2* and *Ptp4a2* and relative expression was calculated using the $2^{-\Delta\Delta CT}$ method in the Bio-Rad CFX Manager 3.1 Software program (Bio-Rad). The number of biological replicates is indicated in each figure legend.

IHC

Formaldehyde-fixed, paraffin-embedded tissue sections were stained for cleaved caspase-3. Formalin-fixed tumor pieces were embedded in paraffin and then sectioned randomly at 4 μm and placed on Superfrost Plus slides (VWR). Sections were dried overnight at 37°C and stored at 4°C until staining. Slides were deparaffinized and endogenous peroxidase was blocked with 0.3% hydrogen peroxidase (VWR) in methanol for 20 minutes. After rehydration, antigen retrieval was performed by boiling slides for 10 minutes in 0.01 mol/L sodium citrate (pH = 6.0; Merck). Non-specific binding was blocked using SuperBlock (Thermo Fisher Scientific, #37537) before overnight incubation at 4°C with rabbit anti-mouse cleaved caspase-3 antibody (clone Asp175, 1:400; Cell Signaling Technology). Thereafter, slides were incubated for 30 minutes at RT with a biotinylated goat anti-rabbit secondary antibody (1:200; Agilent, #E0432), followed by incubation with avidin–biotin complex (VECTASTAIN Elite ABC HRP Kit; Vector Laboratories). Peroxidase activity was detected using the 2-component liquid DAB+ system (Agilent, #K346711–2) according to the manufacturer's instructions for 5 minutes. Slides were counterstained with hematoxylin (Sigma-Aldrich, #H3136), dehydrated, and mounted using Entellan (Sigma-Aldrich, #1.07960). After drying, slides were scanned using the 3DHistech Pannoramic 350 and images were obtained using Caseviewer version 2.4. The DAB signal was quantified using ImageJ software. Control sections were processed in parallel but without incubation with the primary antibody. No labeling was observed in the control sections.

IFNγ ELISA

Sorted Reo $\mu1_{133-140}$ Tm^+ or Reo $\mu1_{422-430}$ Tm^+ cells (2,000 cells/well of a round-bottom 96-wells plate) were cocultured with PMA (20 ng/mL) and ionomycin (1 μg/mL) or Reo-infected TC1 cells (20,000 cells/well). In some wells, NAb-containing plasma from Reo-preexposed mice (1:1,000 dilution) was added. After 48 hours of incubation, supernatants were harvested. For ELISA, Nunc MaxiSorp plates (Corning) were coated with purified rat anti-mouse IFNγ (BD Pharmingen, #551309) in sodium carbonate/sodium bicarbonate coating buffer (pH 9.6) overnight at 4°C and then blocked with PBS/1% BSA/0.05% Tween-20 (Merck) for 1 hour at 37°C. After washing with wash buffer (PBS/0.05% Tween-20), 100 μL of supernatant was added and incubated for 2 hours at RT. The standard curve was prepared using recombinant mouse IFNγ (BioLegend, #575302). After washing, biotinylated rat anti-mouse IFNγ (BD Pharmingen, #551506) was applied for 1 hour at RT, followed by poly-Streptavidin–HRP conjugate (Sanquin, the Netherlands, #M2051) for 1 hour at RT. After washing, 50 μL of TMB (3,3′,5,5′-Tetramethylbenzidine; Sigma–Aldrich, #T0440) was added and the reaction was quenched by the addition of 50 μL 2 mol/L H_2SO_4 (Merck). Absorbance was measured at 450 nm using a SpectraMax iD3 multi-mode plate reader (Molecular Devices).

Statistical analysis

Group size was calculated using the PS: Power and Sample Size Calculation program (Vanderbilt University, version 3.1.6; ref. 32). For experiments where tumor growth was the experimental read-out, mice were excluded when tumor engraftment was not successful (1% of all tumor engraftments). For qRT-PCR analysis, samples were excluded when RNA concentration and purity were too low (<75 ng/μL). For flow cytometry data, tumor samples were excluded when macroscopic evidence for draining lymph node contamination was present.

All graphs were prepared and statistical analyses were performed using the GraphPad Prism software (version 8). All data represent

mean±SEM and key observations are based upon multiple experiments with similar results. For the comparison of two groups, an unpaired *t* test was used. For comparing multiple groups versus PBS treatment or negative control, a one-way ANOVA, including Dunnett's *post hoc* test was performed. For comparing multiple groups with each other, a one-way ANOVA, including the Tukey *post hoc* test was used. To compare differences in average tumor growth, an ordinary two-way ANOVA with Tukey *post hoc* test was used. IC_{50} values were calculated using nonlinear regression analysis. Survival between groups was compared using Kaplan–Meier curves and the statistical Log-rank test (Mantel–Cox). More information regarding the statistical tests used can be found in the individual figure legends. Significance levels are labeled with asterisks, with *, $P < 0.05$; **, $P < 0.01$; ***, $P < 0.001$; and ****, $P < 0.0001$. Non-significant differences are indicated by ns.

Data availability

The data generated in this study are available within the article and its Supplementary Data Files or from the corresponding author upon reasonable request.

Results

Preexisting immunity against Reo is prevalent in the human population

Reo is an emerging anticancer treatment and a promising strategy to enhance the efficacy of immunotherapy. However, various factors, including the presence of preexisting NAbs, might limit its anticancer potential. Before investigating the effect of preexisting immunity on various aspects of Reo therapy, we determined the level of seropositivity against Reo in healthy volunteers and various cohorts of patients with cancer. Using serial dilutions of serum in a virus neutralization assay, we observed that 81.0% of all tested individuals ($n = 100$) carried Reo-specific NAbs (**Fig. 1A** and **B**). The frequency of seropositivity did not differ between healthy volunteers and patients with cancer (**Fig. 1C**), or between male and female individuals (**Fig. 1D**). Reo is known as a "kindergarten" virus and higher seropositivity might thus be expected in younger individuals, but the level of seropositivity was not correlated with age (**Fig. 1E**). Combined, these data confirm that the majority of the human population has been preexposed to Reo, which underscores the relevance of determining the effect of preexposure on the efficacy of Reo-based anticancer therapies.

Preexposure impairs intratumoral Reo infection and the Reo-induced IFN response

To study the role of preexisting immunity on Reo antitumor efficacy, we established an experimental model in which immunocompetent C57BL/6J mice were preexposed to Reo twice with a two-week interval (**Fig. 2A**). This preexposure led to the presence of high levels of NAbs in the circulation (**Fig. 2B** and **C**), as well as $CD8^+$ T cells recognizing the Reo $\mu1_{133–140}$ epitope (**Fig. 2D**; ref. 33). NAb levels remained high over time (Supplementary Fig. S3). Western blot analysis using the plasma of preexposed mice as the primary antibody source revealed that Reo-specific antibodies also predominantly recognize the μ1 protein (**Fig. 2E**), suggesting that immunodominant Reo-specific T- and B-cell responses are both directed to the same viral protein.

As a first step of Reo anticancer efficacy, we investigated whether Reo infection of the tumor was affected by preexisting immunity. After preexposure, mice were engrafted with KPC3 tumors and received intratumoral Reo injections when tumors were palpable. On day 5 post Reo treatment, mice were sacrificed for intratumoral analysis. The quantity of intratumoral genomic copies of the Reo S4 segment was significantly decreased in preexposed mice compared with naive mice, implying impaired viral infection (**Fig. 2F**). Concomitantly, the expression of a panel of ISGs, including *Ifit-1, Ifit-2*, and *Ifit-3*, as well as T-cell attracting chemokines *Cxcl10* and *Cxcl11*, was lower in tumors of preexposed mice (**Fig. 2G**). The expression of chemokine *Cxcl9* appeared to be less affected. Altogether, we concluded that Reo preexposure is associated with a strong decrease in Reo genomic copies and ISG expression in tumors upon Reo treatment.

Reo-specific NAbs impair the anticancer efficacy of Reo monotherapy

We next specifically investigated the effect of NAbs induced by Reo preexposure. μMT mice, which lack B cells and thus cannot produce antibodies (Supplementary Fig. S4A–S4D), were exposed to Reo but succumbed to weight loss (Supplementary Fig. S4E) 2 weeks after inoculation, suggesting that Reo replication was uncontrolled in the absence of NAbs. Then, a tumor challenge experiment was performed in a small number of immunocompromised NSG mice that are also B-cell deficient. Similarly, Reo-exposed NSG mice succumbed to weight loss, and high numbers of Reo genomic copies were detected in tumors, livers, hearts, and plasma of these mice, indicating viremia in the absence of NAbs (Supplementary Fig. S4F–S4I). These data and similar observations by others (34–36) demonstrate that NAbs are necessary to prevent uncontrolled Reo infection in mice.

We then investigated the effect of strongly decreased, but not completely absent, levels of NAbs on Reo infection in immunocompetent C57BL/6J mice by injection of CD20-specific antibodies to deplete B cells (**Fig. 3A**). Indeed, although the depletion of B cells was efficient in blood (Supplementary Fig. S5A and S5B), neutralization assay (**Fig. 3B**) and Western blot analysis (Supplementary Fig. S6) showed that residual levels of NAbs were still present in the plasma of preexposed mice. These low NAb levels were sufficient to protect mice from Reo-induced pathology but hampered Reo infection (**Fig. 3C**) and ISG expression (**Fig. 3D**) in the tumor. Even the intratumoral administration of a 10-fold higher dose of Reo to preexposed mice did not increase the presence of genomic Reo S4 copies (**Fig. 3D**), demonstrating that even low systemic levels of NAbs significantly hamper intratumoral Reo infection and ISG expression. This suggests that achieving effective infection in most patients will be difficult, including those with low NAb levels.

Because of the crucial role of $CD4^+$ T cells in establishing effective class-switched B-cell responses, we depleted $CD4^+$ T cells during Reo preexposure as another way to influence NAb levels (**Fig. 3E**; Supplementary Fig. S5C and S5D). Depletion of $CD4^+$ T cells during preexposure, but not $CD8^+$ T cells or NK cells, completely abrogated NAb production (**Fig. 3F**) and significantly increased genomic Reo S4 copies (**Fig. 3G**) and the expression of ISGs (**Fig. 3H**) in the tumor upon intratumoral Reo treatment. Combined, these data show that the presence of Reo-specific NAbs impairs infection and ISG expression, even when Reo is injected directly into tumors.

Because circulating NAbs can already be detected five days after intratumoral Reo administration (Supplementary Fig. S7), these therapy-induced NAbs might hinder the therapeutic potency of intratumoral Reo treatment even at early time points. Therefore, we next evaluated the therapeutic potency of oncolytic Reo in the absence of NAbs in KPC3-bearing B cell–deficient μMT mice (**Fig. 4A**). Intratumoral injection with Reo created a therapeutic time window that allowed us to study the role of treatment-induced NAbs before the loss of bodyweight occurred (**Fig. 4B**). Reo treatment in μMT mice was

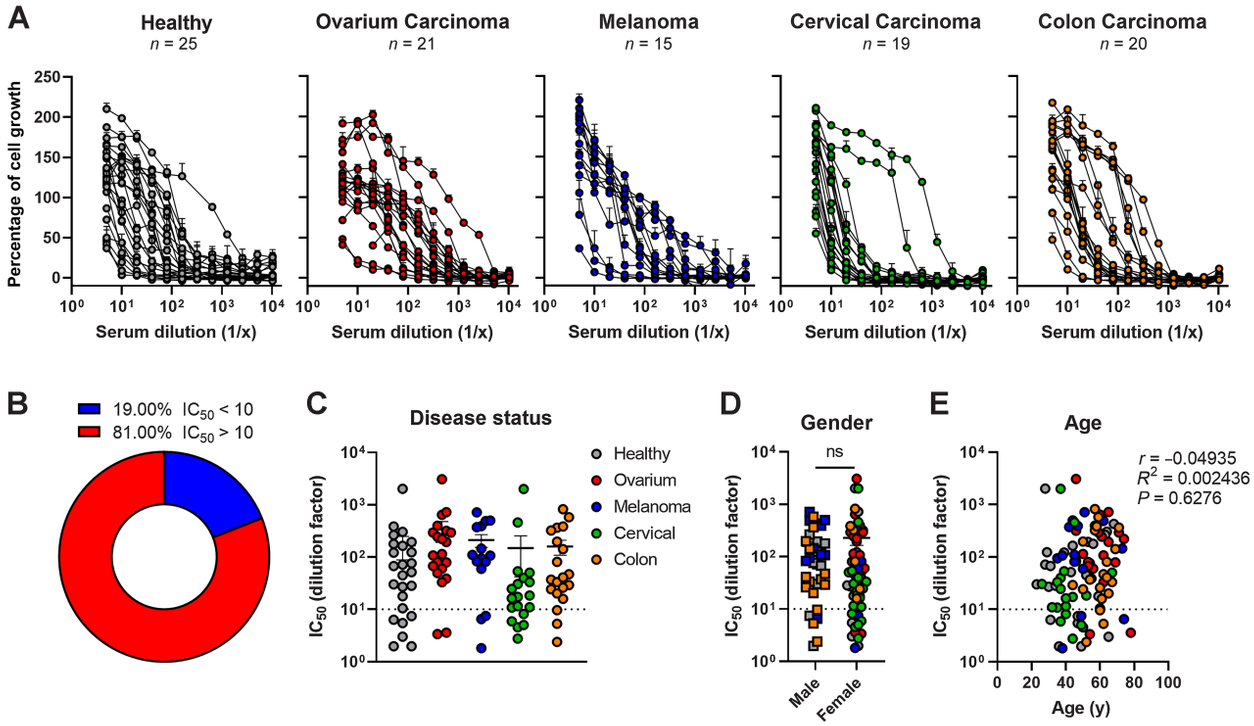

Figure 1.

Preexisting immunity against Reo is prevalent in the human population. **A,** Individual serum samples from healthy volunteers or patients with cancer with different primary tumors were subjected to a Reo neutralization assay. The percentage of cell growth is calculated by normalizing for Reo only (0% viable) and Mock (100% viable). Number of tested sera in each cohort is indicated below the title of each graph. Error bars represent SD of technical replicates. **B,** The percentage of all individuals that tested seropositive (IC_{50} > 10) or seronegative (IC_{50} < 10) for Reo. **C,** Comparison of IC_{50} values between healthy volunteers and cancer patient cohorts. **D,** Comparison of IC_{50} values between male and female individuals. **E,** Correlation analysis between IC_{50} values of individuals and corresponding age in years. IC_{50} values in (**B–E**) were calculated using nonlinear regression analysis. Differences between groups in (**C**) were determined using a Kruskal–Wallis test with the Dunn multiple comparisons test. Differences between groups in (**D**) were determined using an unpaired *t* test with Welch correction, and correlation between IC_{50} values and age in (**E**) was determined by calculating the Pearson correlation coefficient (*r*). Data represent mean±SEM. ns, not significant.

associated with significant decreases in tumor volumes, which were not observed in fully immunocompetent, Reo-treated C57BL/6J mice (**Fig. 4C**). Similar levels of Reo S4 copies could be found in Reo-treated tumors from μMT mice and C57BL/6J mice, even though tumors from μMT mice were smaller in size (**Fig. 4D**). In addition, the expression of ISGs (**Fig. 4E**) and the level of apoptosis, measured by cleaved caspase-3, was higher in tumors from Reo-treated μMT mice compared with those from Reo-treated C57BL/6J mice (**Fig. 4F** and **G**).

To further show that NAbs impair the antitumor effect of Reo therapy, a NAb transfer experiment was performed. KPC3-bearing NSG mice received plasma from naive C57BL/6J mice or NAb-containing plasma from preexposed C57BL/6J mice. The NAb containing plasma was administered at 2 different doses, and mice were subsequently treated intratumorally with Reo (**Fig. 4H**; Supplementary Fig. S8). Even though NAbs were only detected after infusion of the high dose NAb-containing plasma (**Fig. 4I**) and NAbs did not reduce the genomic Reo S4 copies in tumors (**Fig. 4J**), the transfer of both doses of NAbs reduced the Reo-induced expression of ISGs (**Fig. 4K**) and the level of cleaved caspase-3 (**Fig. 4L** and **M**) in the tumor. Moreover, the transfer of NAb-containing plasma, but not naive plasma, completely neutralized the Reo-induced antitumor effect (**Fig. 4N**). These combined results show that Reo can have profound antitumor efficacy, but its use as an oncolytic agent is impaired by the presence of NAbs, even at low levels.

Preexposure does not affect the Reo-induced intratumoral influx or activation of T cells

Current clinical efforts aim to use Reo not solely as an oncolytic agent, but also as an immunostimulatory agent, especially to induce the intratumoral influx of T cells that can be harnessed by T-cell–based immunotherapeutic strategies (37–39). Therefore, we next studied whether the intratumoral T-cell influx induced by Reo therapy is affected by Reo preexposure. Immunocompetent C57BL/6J mice were preexposed to Reo, engrafted with KPC3 tumors, treated intratumorally with Reo and then the frequency, specificity, and effector function of intratumoral T cells was analyzed (**Fig. 5A**). We observed that the Reo-induced influx of $CD8^+$ T cells was not affected by preexposure to Reo (**Fig. 5B** and **C**). Equally, the intratumoral influx of $CD8^+$ T cells did not differ between Reo-treated μMT mice and Reo-treated C57BL/6J mice, demonstrating that T-cell influx is not affected by the presence or absence of NAbs (Supplementary Fig. S9A and S9B). This might be related to the moderate expression of *Cxcl9* that was still present in tumors of preexposed mice (**Fig. 2G**). In contrast, the Reo-induced intratumoral influx of NK cells was lower in preexposed C57BL/6J mice and higher in Reo-treated μMT mice, suggesting that the influx of NK cells was more influenced by the presence of NAbs or ISG expression than the influx of T cells (**Fig. 5D**; Supplementary Fig. S9C).

Although the intratumoral influx of $CD8^+$ T cells was not affected by the presence of NAbs, the proportion of T cells recognizing our

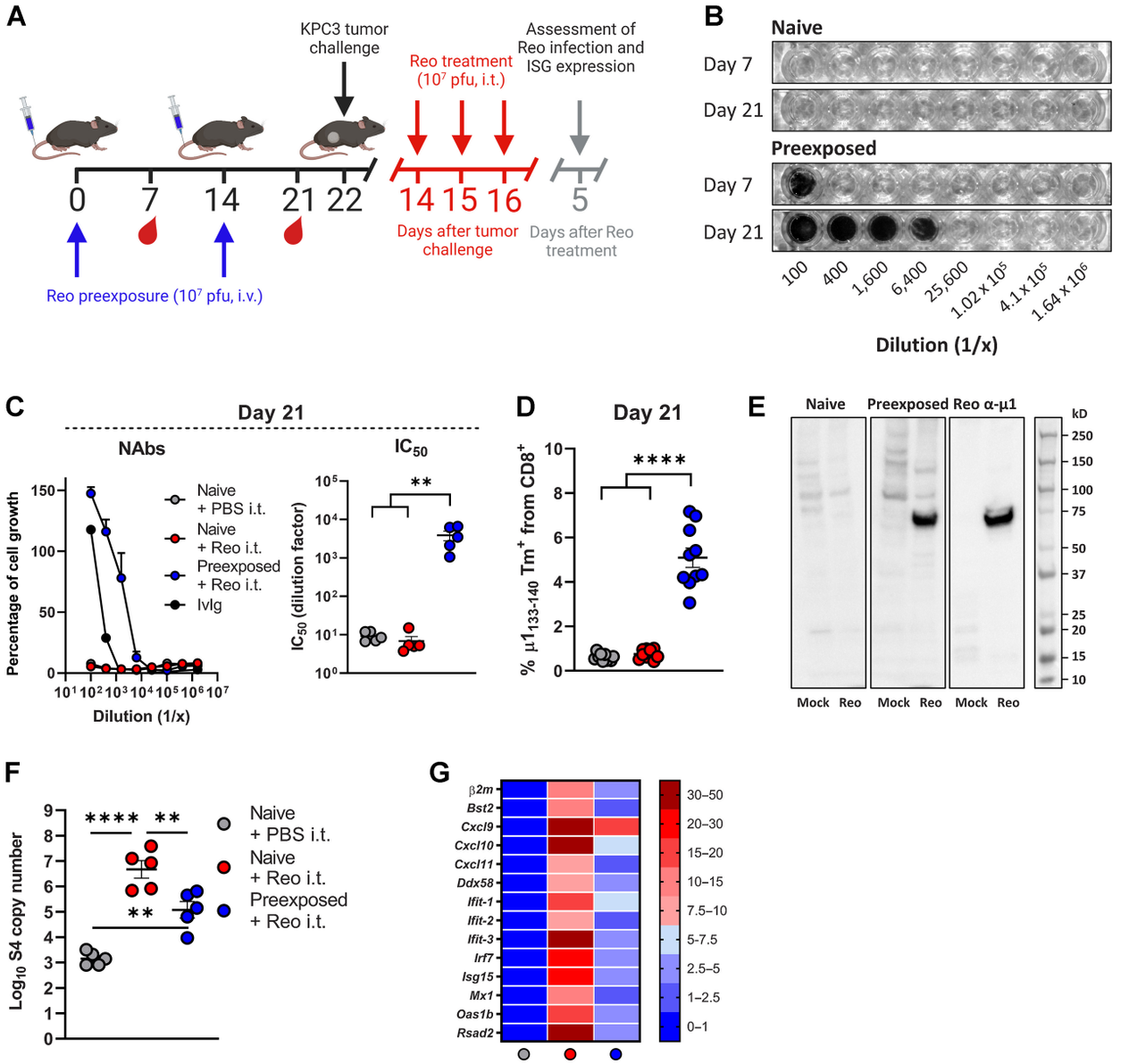

Figure 2.

Preexposure impairs Reo infection and the Reo-induced IFN response. **A,** Overview of experiment described in (**B–G**). Male C57BL/6J mice ($n = 5$/group) were preexposed by intravenous (i.v.) injection of Reo (10^7 plaque-forming units (pfu)/injection) on days 0 and 14. Blood was drawn on days 7 and 21 for interim analysis. After preexposure, mice were subcutaneously inoculated with KPC3 cells (1×10^5/mouse) and received intratumoral (i.t.) Reo injections (10^7 pfu/injection) on indicated days. Tumors were harvested 5 days after Reo administration for *ex vivo* analysis. **B,** Representative pictures of crystal violet-stained 911 cells after subjection to a neutralization assay with diluted plasma from naive or preexposed mice. **C,** Reo neutralization assay. Average dilution curves using plasma from naive or preexposed mice and individual IC_{50} values on day 21. **D,** Frequency of Reo-specific $\mu1_{133-140}$ tetramer $(Tm)^+CD8^+$ T cells in the circulation on day 21. Data are pooled from two individual experiments. **E,** Western blot of Mock or Reo-infected 911 cell lysates using antibodies against the Reo μ1 protein or plasma of preexposed mice as primary antibody source. **F,** Intratumoral presence of genomic copies of Reo S4 segment, as measured by qRT-PCR. **G,** Heat map depicting relative expression of various IFN response genes on day 5, as determined by qRT-PCR on bulk tumor RNA. IC_{50} values in (**C**) were calculated using nonlinear regression analysis. Differences between groups in (**C**, **D**, and **F**) were determined using an ordinary one-way ANOVA with the Tukey *post hoc* test. Data represent mean±SEM. **, $P < 0.01$; ****, $P < 0.0001$. (**A,** Created with BioRender.com.)

previously identified Reo $\mu1_{133-140}$ epitope (in red) was strongly diminished (Supplementary Fig. S10A). Intratumoral $CD8^+$ T cells in preexposed mice were still Reo-specific (Supplementary Fig. S10B) but now recognized another epitope ($\mu1_{422-430}$, in blue; **Fig. 5E**; Supplementary Fig. S10C and S10D). Further analysis of these two Reo-specific $CD8^+$ T-cell populations using tetramers (**Fig. 5F**), revealed different kinetics (**Fig. 5G**) and confirmed that especially in tumors of preexposed mice, the frequency of $\mu1_{422-430}$-specific $CD8^+$ T cells dominated over the frequency of those recognizing the $\mu1_{133-140}$ epitope (**Fig. 5H**).

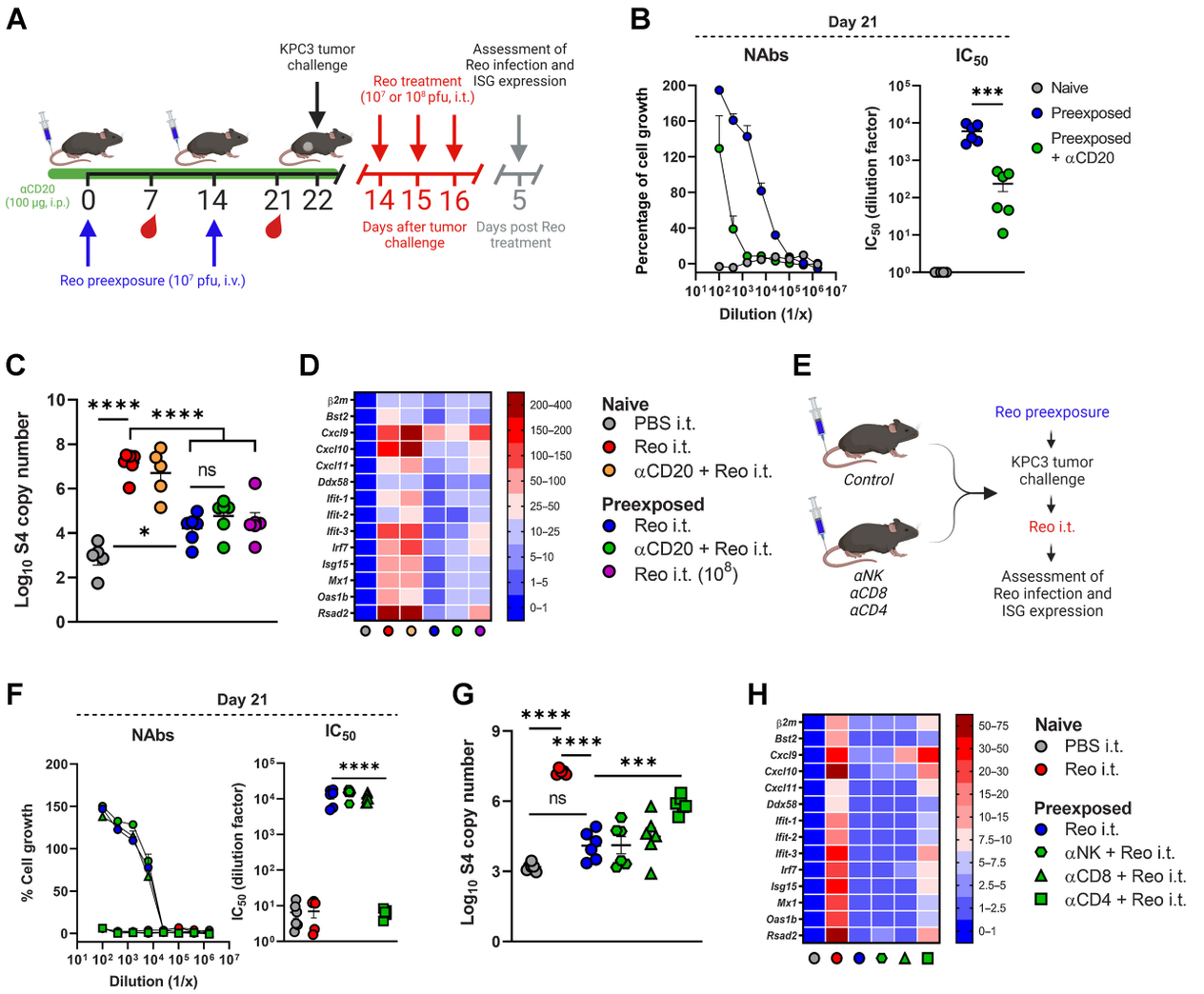

Figure 3.

Preexposure-induced Reo-specific NAbs impair Reo infection and ISG expression in the tumor. **A,** Overview of experiment described in (**B–D**). Male C57BL/6J mice ($n = 5$–7/group) were preexposed by intravenous (i.v.) injection of Reo (10^7 plaque-forming units (pfu)/injection) on days 0 and 14. Depletion of B cells [αCD20, 100 μg/injection, intraperitoneally (i.p.)] was initiated on days −5 and −1 and maintained weekly during the preexposure period. Blood was drawn on days 7 and 21 for interim analysis. After preexposure, mice were subcutaneously inoculated with KPC3 cells (1×10^5/mouse) and received intratumoral (i.t.) Reo injections (10^7 of 10^8 pfu/injection) on indicated days. Tumors were harvested 5 days after Reo administration for *ex vivo* analysis. **B,** Reo neutralization assay. Average dilution curves using plasma from indicated groups and individual IC_{50} values on day 21. **C,** Intratumoral presence of genomic copies of Reo S4 segment, as measured by qRT-PCR. **D,** Heat map depicting relative expression of various IFN response genes on day 5, as determined by qRT-PCR. **E,** Design of experiment described in (**F–H**). Experiment was executed exactly as described in (**A**), but male C57BL/6J mice ($n = 6$/group) received αNK, αCD8, or αCD4 (100 μg/injection, i.p.) during the preexposure period. **F,** Reo neutralization assay. Average dilution curves using plasma from indicated groups and individual IC_{50} values on day 21. **G,** Intratumoral presence of genomic copies of Reo S4 segment, as measured by qRT-PCR. **H,** Heat map depicting relative expression of various IFN response genes on day 5, as determined by qRT-PCR. IC_{50} values in (**B**) and (**F**) were calculated using nonlinear regression analysis. To determine differences between groups in (**B, D,** and **F**), an ordinary one-way ANOVA with Tukey *post hoc* test was used. Data represent mean±SEM. *, $P < 0.05$; ***, $P < 0.001$; ****, $P < 0.0001$; ns, not significant. (**A** and **E,** Created with BioRender.com.)

To determine whether this shift in frequency of Reo-specific T-cell populations was specifically caused by Reo preexposure, we preexposed mice to another OV, VSV (**Fig. 5I**). VSV preexposure induced high levels of VSV-specific NAbs and VSV $NP_{52–59}$ $CD8^+$ T cells, whereas Reo-specific NAbs and Reo-specific $CD8^+$ T cells were absent (Supplementary Fig. S11). Upon intratumoral Reo injection in VSV-preexposed or Reo-preexposed mice, the shift in the frequency of Reo-specific T-cell populations could only be observed in Reo-preexposed mice whereas their distribution in VSV-preexposed mice was similar to non-preexposed mice (**Fig. 5J**; Supplementary Fig. S12). We conclude that the shift in frequency of Reo-specific $CD8^+$ T cells is caused specifically by Reo preexposure.

Because it has been previously shown that circulating myeloid cells can internalize and process Reo particles that are complexed with Reo-specific NAbs (14), we set out to investigate the role of myeloid cells in the observed dominance of $\mu1_{422–430}$-specific $CD8^+$ T cells over $\mu1_{133–140}$-specific $CD8^+$ T cells in preexposed mice, compared with naive mice that do not have circulating NAbs. First, we

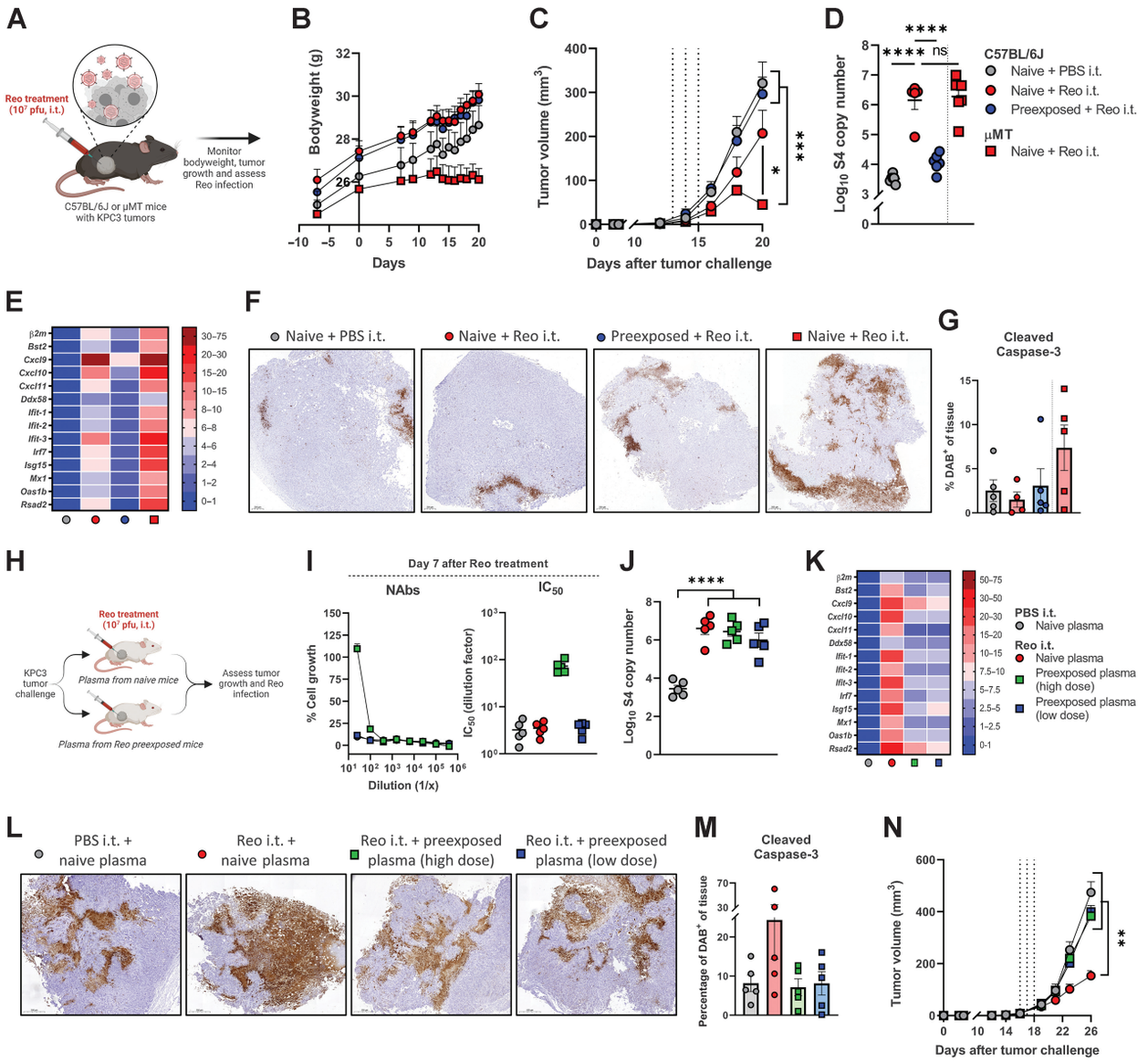

Figure 4.

Reo-specific NAbs abrogate the antitumor efficacy of Reo monotherapy. **A,** Overview of experiment described in (**B–G**). Male C57BL/6J or μMT mice ($n = 6$/group) were subcutaneously inoculated with KPC3 cells (1×10^5/mouse) and received intratumoral (i.t.) Reo injections (10^7 pfu/injection) on days 13–15. Mice were sacrificed 7 days after Reo administration for *ex vivo* analysis. **B,** Average bodyweight curves. **C,** Average tumor volume curves. **D,** Intratumoral presence of genomic copies of Reo S4 segment, as measured by qRT-PCR. **E,** Heat map depicting relative expression of various IFN response genes, as determined by qRT-PCR. **F,** Representative images obtained from IHC staining of KPC3 tumors for apoptosis marker cleaved caspase-3; scale bar equals 200 μm. **G,** Quantification of positive DAB signal in sections stained for cleaved caspase-3. **H,** Overview of experiment described in (**I–N**). Male and female NSG mice ($n = 5$/group) were subcutaneously inoculated with KPC3 cells (1×10^5/mouse) and received intratumoral (i.t.) Reo injections (10^7 pfu/injection) on days 16–18. Plasma from preexposed C57BL/6J mice was injected intraperitoneally, 2x/wk. Mice were sacrificed 10 days after Reo administration for *ex vivo* analysis. **I,** Reo neutralization assay. Average dilution curves and individual IC_{50} values using plasma from indicated groups, harvested on day 7 after i.t. Reo administration. **J,** Intratumoral presence of genomic copies of Reo S4 segment, as measured by qRT-PCR. **K,** Heat map depicting relative expression of various IFN response genes in tumors, as determined by qRT-PCR. **L,** Representative images obtained from IHC staining of KPC3 tumors for apoptosis marker cleaved caspase-3; scale bar equals 500 μm. **M,** Quantification of positive DAB signal in sections stained for cleaved caspase-3. **N,** Average tumor volume curves. IC_{50} values in (**I**) were calculated using nonlinear regression analysis. Differences between groups in (**C** and **N**) were determined using an ordinary two-way ANOVA with the Tukey *post hoc* test, and an ordinary one-way ANOVA with the Tukey *post hoc* test was used to determine differences between groups in (**D** and **J**). Data represent mean±SEM. *, $P < 0.05$; **, $P < 0.01$; ***, $P < 0.001$; ****, $P < 0.0001$; ns, not significant. (**A** and **H,** Created with BioRender.com.)

investigated the number and phenotype of circulating myeloid cells during Reo preexposure. We observed small shifts in frequencies of $CD11b^+$, $CD11c^+$, and $Ly6C^+$ populations but no changes in phenotype (Supplementary Fig. S13). Next, we depleted phagocytic myeloid cells using clodronate liposomes during Reo preexposure (**Fig. 5K**; Supplementary Fig. S14) and assessed the frequency of both Reo-specific $CD8^+$ T-cell populations in the circulation. The frequency of $\mu1_{133-140}$-specific $CD8^+$ T cells was significantly higher in clodronate liposome-treated, Reo-preexposed mice compared with the Reo-preexposed group without clodronate liposomes, whereas the frequency of $\mu1_{422-430}$-specific $CD8^+$ T cells was comparable between groups (**Fig. 5L**). Because NAb levels in clodronate liposome-treated mice were similar compared with preexposed-mice without clodronate liposomes (**Fig. 5M**), these data suggest that it is not NAbs themselves, but the uptake of Reo/Nab particles by phagocytic myeloid cells influences the Reo-specific T-cell repertoire.

Finally, we investigated the phenotype of both Reo-specific $CD8^+$ T-cell populations. In the tumor, both Reo-specific $CD8^+$ T-cell populations exhibited a similar effector phenotype, which did not differ between Reo-treated naive and preexposed mice (**Fig. 5N**), and a similar capacity to produce IFNγ upon non-specific stimulation with PMA/ionomycin or upon specific stimulation with Reo-infected target cells (**Fig. 5O**). In addition, their recognition of Reo-infected target cells was not impaired when NAb-containing plasma from preexposed mice was added to the system. Altogether, these data demonstrate that the intratumoral presence of functional T cells is not affected by preexposure to Reo.

Combined Reo and T cell–based immunotherapy retains its efficacy in preexposed mice

Because the total Reo-induced influx and activation of $CD8^+$ T cells was not impaired in preexposed mice, we hypothesized that the combination of Reo and T-cell–based immunotherapy would still be effective in this setting. We first investigated the efficacy of Reo and CD3xTRP1-bsAb therapy (Reo&CD3-bsAbs) in the KPC3.TRP1 tumor model (**Fig. 6A**). As demonstrated before, preexposure induced high levels of NAbs (**Fig. 6B**) and the presence of Reo-specific T cells (**Fig. 6C**) in the circulation. We treated both naive and preexposed mice bearing KPC3.TRP1 tumors with Reo&CD3-bsAbs and observed that tumors of all combination-therapy treated mice regressed in volume, irrespective of their preexposure status (**Fig. 6D**). As demonstrated before, CRs do not occur in this model as therapy-induced selective expansion of TRP1-negative tumor cells prevents full cures (3). Although the survival time after Reo&CD3-bsAbs was decreased in preexposed mice compared with naive mice (**Fig. 6E**), these data demonstrate that Reo&CD3-bsAb therapy is still effective in a preexisting immunity setting.

To assess the role of Reo preexisting immunity in a different combinatorial immunotherapeutic strategy that could induce complete tumor clearance, we used the chemically induced preclinical colon cancer model MC38, which shows a PR to checkpoint blockade therapy in the form of anti–PD-L1 (αPD-L1; ref. 40). We first assessed whether Reo was able to enhance the efficacy of αPD-L1. Reo was administered intratumorally on days 8, 11, and 14 after tumor challenge, and αPD-L1 therapy was applied intraperitoneally on the same days (**Fig. 6F**). Although αPD-L1 alone delayed tumor growth and induced complete tumor clearance in 20% of animals, Reo and αPD-L1 combination therapy (Reo&αPD-L1) led to tumor clearance in 50% of animals (**Fig. 6G** and **H**). We concluded that the combination of Reo&αPD-L1 was very effective in the MC38 tumor model, and subsequently investigated the impact of preexposure to Reo on its efficacy (**Fig. 6I**). Similar to what was observed for Reo&CD3-bsAb therapy, preexposure to Reo (Supplementary Fig. S15) did influence the efficacy of Reo&αPD-L1 therapy, but complete tumor clearance could still be observed in 40% of preexposed mice (**Fig. 6J** and **K**). These data indicate that Reo preexposure does not preclude the use of Reo and T cell–based combination therapy for effective tumor control.

Reo-based combination therapy remains effective upon repeated systemic administration

Given that preexposure does not hamper the efficacy of Reo-based combination therapies when Reo is administered intratumorally, we next investigated the efficacy of Reo-based combination therapy in a more clinically relevant setting. In the clinic, intravenous administration of Reo is preferred over intratumoral administration, because it limits patients' discomfort and allows for the simultaneous targeting of multiple tumor lesions, irrespective of their location. In addition, patients are commonly treated with repeated infusions, which will result in multiple boosting events of Reo-directed immunity that might impair therapeutic efficacy. We therefore investigated the consequences of repeated intravenously Reo infusions on Reo infection and the Reo-induced influx of immune cells (**Fig. 7A**). For this experiment, the clinical-grade formulation of Reo, named pelareorep (Pela in graphs), was used. Pelareorep is currently under investigation in multiple clinical trials as part of combinatorial approaches, including T cell–based immunotherapy, and has shown promising results (41, 42).

Repeated intravenous pelareorep injections impaired the presence of virus in tumors (**Fig. 7B**). Although Reo S4 genomic copies could be found in tumors of mice that received only 1 injection with pelareorep, this greatly diminished after multiple infusions. A similar pattern was observed for the expression of ISGs (**Fig. 7C**). Although the frequency of NK cells decreased after more than one infusion (**Fig. 7D**), the frequency of intratumoral $CD8^+$ T cells remained constant over time after repeated intravenous pelareorep injections (**Fig. 7E**). We next investigated whether the combination therapy of intravenously administered pelareorep combined with CD3xTRP1-bsAbs (CD3-bsAbs) would still be effective. We compared the efficacy of intravenous pelareorep and CD3-bsAbs administered as multiple cycles with a 5-day interval, with our previously defined regimen that comprises 1 cycle of 3 consecutive virus infusions followed by CD3-bsAb administrations (**Fig. 7F**; ref. **3**). Both regimens were equally effective (**Fig. 7G** and **H**), demonstrating that systemic and repeated Reo administration is not a barrier to the antitumor efficacy of combined Reo and T cell–based immunotherapy. Altogether, these data demonstrate that the use of Reo as an oncolytic agent is hampered by the presence of NAbs, but T cells are still attracted toward the tumor and combined Reo and T cell–based immunotherapy remained effective.

Discussion

Here, we tackled an important topic of debate in the field of OV therapy, by investigating the impact of preexisting immunity, in particular the role of Nabs, on the antitumor efficacy of Reo. Our data demonstrate that preexposure-induced Reo-specific NAbs are detrimental to Reo infection and Reo-induced tumor control when used as monotherapy. In contrast, the Reo-induced influx of T cells was not affected by NAbs and Reo-based combinatorial immunotherapy remained effective in preexposed mice.

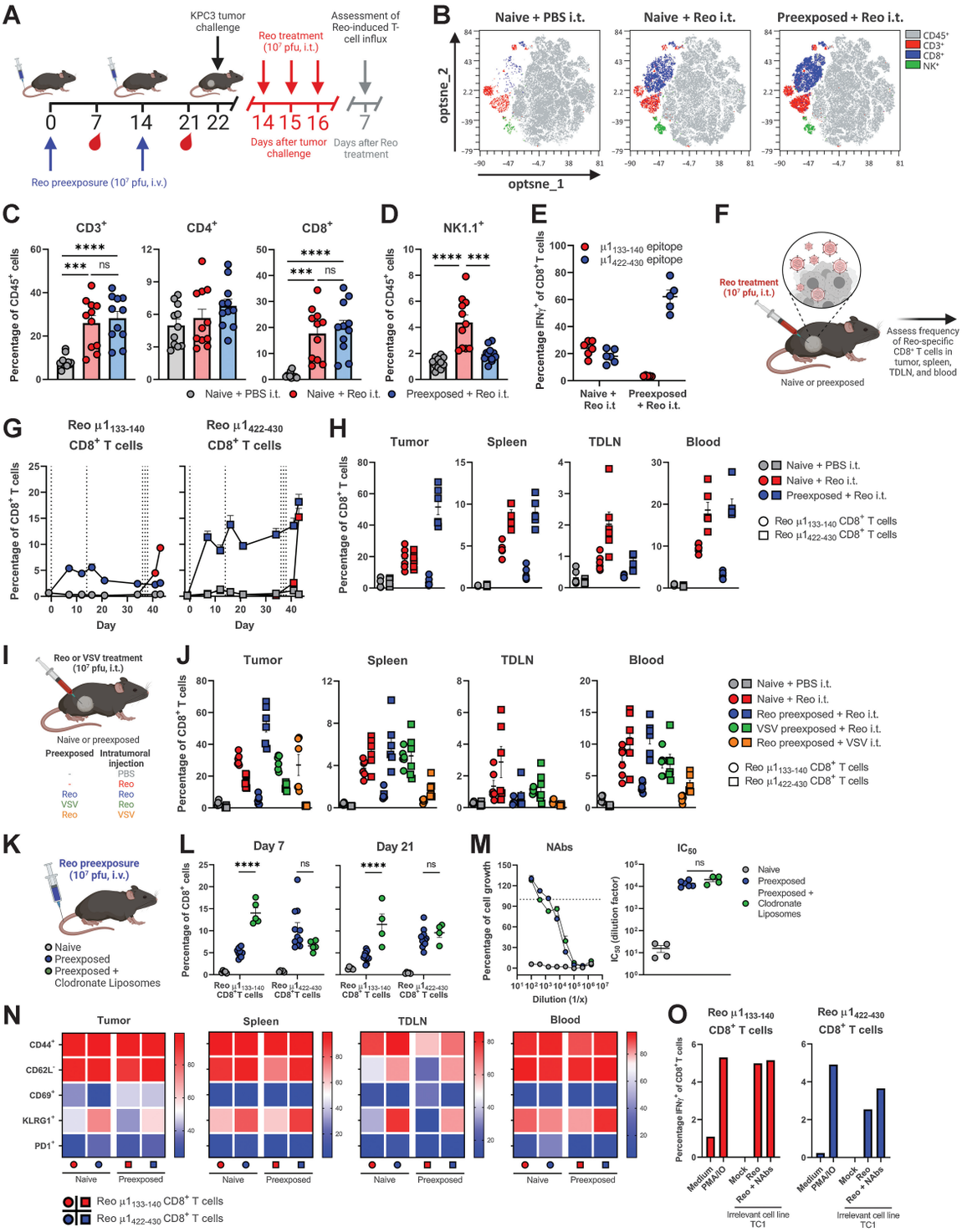

Figure 5.

Preexposure does not affect the Reo-induced intratumoral influx or activation of T cells but shifts the frequency of Reo-specific T-cell populations. **A,** Overview of experiment described in (**B–E**). Male C57BL/6J mice (n = 5–6/group) were preexposed by intravenous (i.v.) injection of Reo (10^7 plaque-forming units (pfu)/injection) on days 0 and 14. After preexposure, mice were subcutaneously inoculated with KPC3 cells (1×10^5/mouse) and received intratumoral (i.t.) Reo injections (10^7 pfu/injection) on days 14–16. Tumors were harvested 7 days after Reo administration for *ex vivo* analysis. **B,** Opt-SNE plots highlighting the intratumoral presence of $CD3^+$, $CD8^+$ T cells, and NK cells after indicated treatments. A total of 1×10^5 $CD45^+$ cells were subsampled from each sample. **C,** Intratumoral frequency of $CD3^+$, $CD4^+$, and $CD8^+$ T cells within $CD45^+$ immune cells. **D,** Intratumoral frequency of NK cells within $CD45^+$ immune cells. (*Continued on the following page.*)

It currently remains unknown why the Reo-induced T-cell influx remained unaffected by preexposure, even though the copy numbers of Reo and the expression of ISGs in tumors were impaired. However, a similar observation was made in a study where immunocompetent naive or Newcastle disease virus (NDV)-exposed B16.F10-bearing C57BL/6J mice were intratumorally injected with NDV (43). Although viral replication was decreased in preexposed mice, the NDV-induced intratumoral influx of $CD8^+$ T cells was comparable between naive and preexposed animals. In our study, it might be possible that the remaining moderate expression of T cell–attracting chemokine *Cxcl9* in tumors of preexposed mice was sufficient to attract T cells to the tumor. In contrast with *Cxcl10* and *Cxcl11*, which are induced by both type I and type II IFN, *Cxcl9* is only induced by type II IFN, which might contribute to this different expression pattern (44). Furthermore, the expression of ISGs was strongly reduced in the presence of NAbs, but not completely abrogated. Because IFNs are powerful immune mediators, a very moderate IFN response, either induced by Reo itself, incoming T cells or NK cells, or by the transmission of an antiviral state from a few Reo-infected tumor cells to neighboring tumor cells, might have been sufficient to induce T-cell attraction to the tumor (45, 46).

Alternatively, it is possible that administration of Reo to preexposed mice did not completely preclude effective viral infection and ISG expression, but that the presence of Reo, the expression of ISGs, and the subsequent influx of T cells might follow different kinetics in preexposed mice compared with naive mice. The preexisting NAbs will presumably lead to faster clearance of the virus, even upon intratumoral injection. However, a short presence of Reo in the tumor might already have been sufficient to attract and maintain T cells in the tumor, without the need for continued viral presence.

Although the total intratumoral T-cell numbers were not affected by Reo preexposure, we observed a substantial shift in the specificity of the Reo-specific T-cell repertoire. It is known that the presence of NAbs (47) can enhance FcγR-mediated uptake of viral particles by circulating myeloid cells, which might contribute to this observed shift in Reo-specific $CD8^+$ T cells. Indeed, depletion of phagocytic myeloid cells increased the frequency of Reo $\mu1_{133-140}$ $CD8^+$ T cells in Reo preexposed mice, suggesting that the presentation of this epitope is influenced by the presence of NAbs and phagocytes. We speculate that in the absence of NAbs or phagocytes, there is more reovirus available to prime Reo $\mu1_{133-140}$-specific $CD8^+$ T cells, possibly by cDC1s as we demonstrated before (33). It appears that Reo $\mu1_{422-430}$-specific $CD8^+$ T cells are less affected by the presence of NAbs, but the mechanism behind this observation remains to be investigated. Although these observations provide interesting avenues for further research, we conclude here that the impaired Reo infection observed in preexposed mice, or upon repeated intravenous Reo infusions, does not preclude effective intratumoral T-cell influx and thus permits potent antitumor responses upon combinatorial Reo and T cell–based immunotherapy.

The conclusion that NAbs present a barrier for the antitumor efficacy of Reo monotherapy may be surprising, because previous studies suggested that NAbs are beneficial (14, 15). However, the beneficial role of NAbs has only been demonstrated in the context of immune cell carriage. For instance, mechanistic studies have shown that Reo can be taken up and internalized by various immune cells, including human monocytes, DCs, and T cells (13–15, 48, 49). Here, the presence of NAbs can contribute to enhanced uptake, because Reo/NAb complexes are more efficiently internalized by immune cells compared with Reo particles alone. Thus, NAbs might be beneficial specifically when using cellular carriers for Reo delivery to tumors, but the effect of NAbs on the antitumor efficacy of Reo remained unknown. Here, we unequivocally demonstrate that the presence of NAbs restricts the antitumor efficacy of Reo therapy, even when administered intratumorally.

Because a large proportion of the human population, including patients with cancer, has been preexposed to Reo and thus has circulating NAbs, our data may explain why Reo monotherapy has not yet reached optimal efficacy in clinical studies. Still, various approaches, including the above-mentioned use of immune cell carriage, have been proposed to enhance the delivery of Reo particles to tumors in the presence of NAbs (7). For instance, the use of a low dose of the chemotherapeutic drug cyclophosphamide (CPA) leads to the depletion of regulatory T cells and enhanced tumor-specific $CD8^+$ T-cell responses (50, 51), but can also ablate the production of NAbs, leading to enhanced anticancer efficacy of Reo therapy (52, 53). Although these preclinical results were encouraging, compiled data from various Phase I clinical trials demonstrated that the effect of CPA or other chemotherapeutic drugs such as gemcitabine and docetaxel only moderately reduced Reo-specific NAb responses (54). In addition, the use of CPA or other chemotherapeutics to prevent NAb production might only be relevant for individuals who have not been exposed to Reo before, which is a minority of patients. Alternatively, it might be possible to use certain apheresis techniques such as plasma exchange (55) or immunoadsorption (56) in seropositive patients, which are already applied in the context of autoimmune diseases and organ transplants. Especially immunoadsorption ensures rapid removal of specific antibodies from the circulation, and might be performed in seropositive patients before Reo therapy to greatly reduce the level of preexisting NAbs. However, the activation of Reo-specific B cells upon the first therapeutic Reo administration will lead to rapidly emerging new NAbs that will hamper the efficacy of subsequent infusions.

The above-mentioned strategies could be used to reduce, circumvent, or remove NAb responses to increase the efficacy of Reo

(*Continued.*) **E,** Frequency of $IFN\gamma^+$ cells within the intratumoral $CD8^+$ T-cell population after coculture with indicated peptides, as measured with intracellular cytokine staining. **F,** Design of experiment described in (**G–J**). Mice ($n = 6$/group) were preexposed with Reo, inoculated with KPC3 cells, and treated i.t. with Reo as described in (**A**). **G,** Kinetics of Reo-specific $\mu1_{133-140}$ and $\mu1_{422-430}$ tetramer $(Tm)^+CD8^+$ T cells in the circulation. **H,** Frequency of Reo-specific $\mu1_{133-140}$ and $\mu1_{422-430}$ Tm^+CD8^+ T cells in tumor, spleen, TDLN, or blood of naive or preexposed mice after intratumoral Reo administration. **I,** Design of experiment described in (**J**). Mice ($n = 5$–6/group) were preexposed with Reo or VSV, inoculated with KPC3 cells, and treated i.t. with Reo or VSV as described in (**A**). **J,** Frequency of Reo-specific $\mu1_{133-140}$ and $\mu1_{422-430}$ Tm^+CD8^+ T cells in tumor, spleen, TDLN, or blood of naive, Reo-preexposed or VSV-preexposed mice after intratumoral Reo or VSV administration. **K,** Design of experiment described in (**L** and **M**). Mice ($n = 5$–6/group) were preexposed with Reo as described in (**A**) and received clodronate liposomes [1.5 mg every 5 days, intraperitoneally (i.p.)]. **L,** Frequency of Reo-specific $\mu1_{133-140}$ and $\mu1_{422-430}$ Tm^+CD8^+ T cells in blood on days 7 and 21. **M,** Reo neutralization assay. Average dilution curves and individual IC_{50} values using plasma from indicated groups, harvested on day 21. **N,** Heat map showing activation profile of Reo-specific $\mu1_{133-140}$ (red) and $\mu1_{422-430}$ (blue) Tm^+CD8^+ T cells in tumor, spleen, TDLN, or blood. **O,** Production of IFNγ by sorted Reo-specific $\mu1_{133-140}$ or $\mu1_{422-430}$ Tm^+CD8^+ T cells after coculture with indicated targets for 48 hours. In (**C** and **D**), data from two experiments with the same set-up are pooled and differences between groups were determined using an ordinary one-way ANOVA with the Tukey *post hoc* test. Data represent mean±SEM, except in (**J**), where $n = 1$. ***, $P < 0.001$; ****, $P < 0.0001$; ns, not significant. (**A, F, I, K,** Created with BioRender.com.)

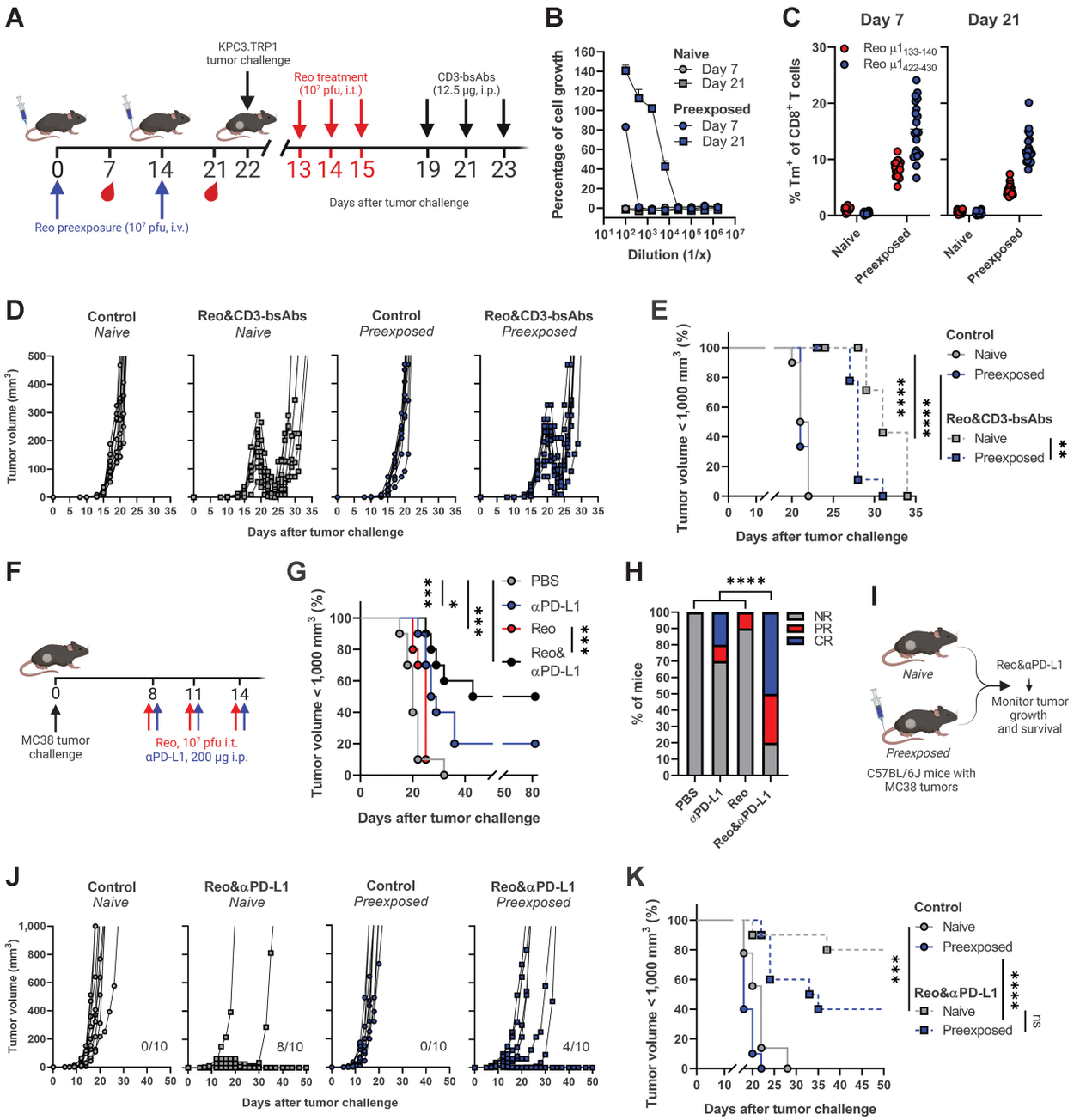

Figure 6.

Combined Reo and T-cell–based immunotherapy retains its efficacy in preexposed mice. **A,** Overview of experiment described in (B–E). Male C57BL/6J mice (n = 10/group) were preexposed by intravenous (i.v.) injection of Reo [10^7 plaque-forming units (pfu)/injection] on days 0 and 14. After preexposure, mice were subcutaneously inoculated with KPC3.TRP1 cells (1×10^5/mouse) and received intratumoral (i.t.) Reo injections (10^7 pfu/injection) on indicated days, followed by intraperitoneal (i.p.) administration of CD3xTRP1-bsAbs (12.5 µg/injection). **B,** Reo neutralization assay. Average dilution curves using plasma harvested on indicated days. **C,** Reo-specific $\mu1_{133-140}$ and $\mu1_{422-430}$ tetramer $(Tm)^+CD8^+$ T cells in the circulation on indicated days. **D,** Individual growth curves of naive or preexposed mice receiving Reo and CD3xTRP1-bsAb (Reo&CD3-bsAb) therapy. **E,** Kaplan–Meier survival graphs of mice after indicated treatments. **F,** Overview of experiment described in (**G** and **H**). Male C57BL/6J mice (n = 10/group) were subcutaneously engrafted with MC38 cells (5×10^5/mouse) and received Reo (i.t., 10^7 pfu/injection) and anti–PD-L1 (αPD-L1; i.p., 200 µg/injection) on day 8, 11 and 14. **G,** Kaplan–Meier survival graphs of mice after indicated treatments. **H,** Frequency of Non-Responders (NR), Partial Responders (PR), or Complete Responders (CR) within each treatment group. **I,** Overview of experiment described in (**J** and **K**). Male C57BL/6J mice (n = 10/group) were preexposed as described in (**A**). After preexposure, mice were subcutaneously inoculated with MC38 cells (5×10^5/mouse) and received Reo and anti–PD-L1 (Reo&αPD-L1) therapy as described in (**F**). **J,** Individual growth curves of naive or preexposed mice receiving Reo&αPD-L1 therapy. Indicated is the number of tumor-free mice in each experimental group. **K,** Kaplan–Meier survival graphs of mice after indicated treatments. Log-rank tests were used to compare differences in survival in (**E, G,** and **K**). The χ^2 test was used to determine statistical differences in response in (H). Data represent mean±SEM. *, $P<0.05$; **, $P<0.01$; ***, $P<0.001$; ****, $P<0.0001$; ns, not significant. (**A, F, I,** Created with BioRender.com.)

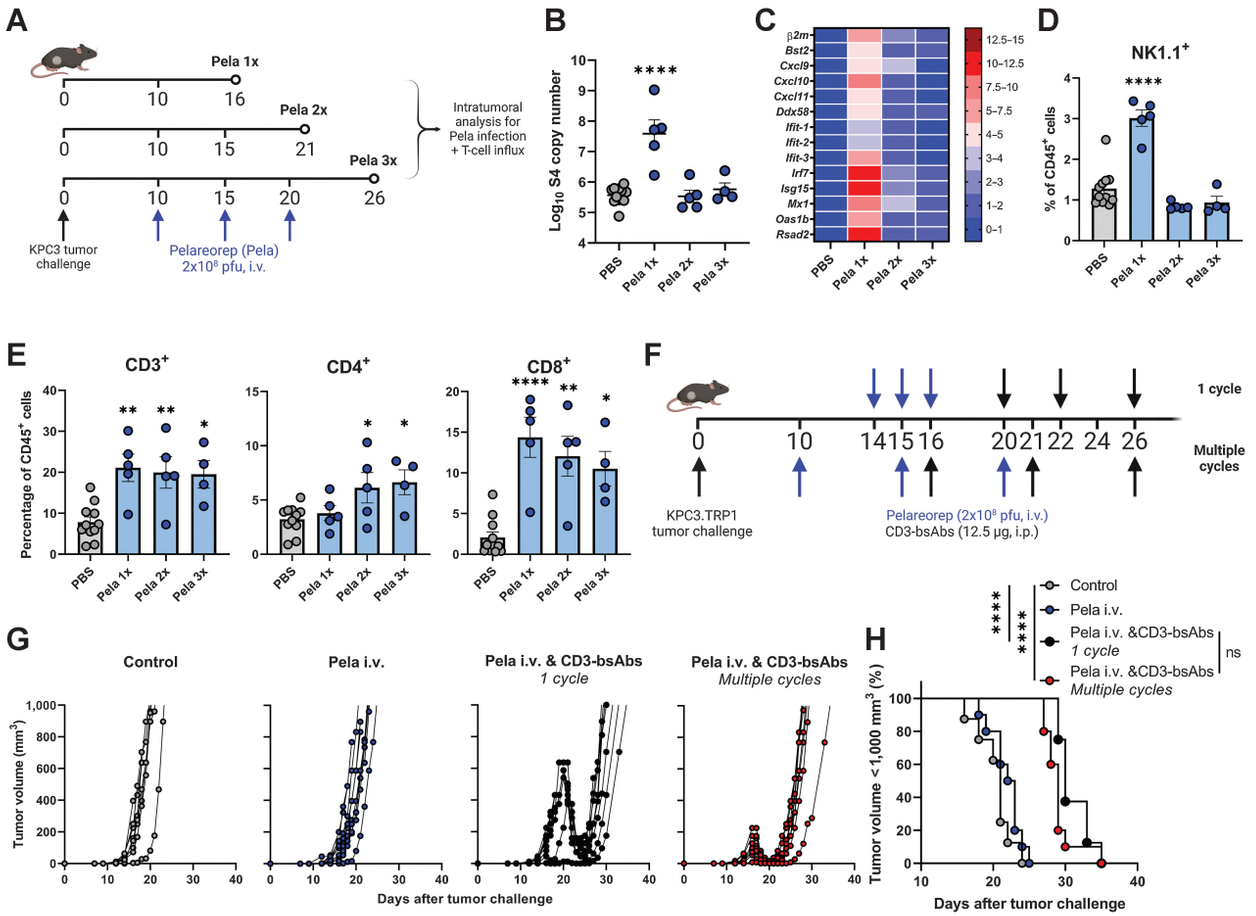

Figure 7.

Reo-based combination therapy remains effective upon repeated systemic administration. **A,** Overview of experiment described in (**B–E**). Male C57BL/6J mice (n = 5/group) were subcutaneously inoculated with KPC3 cells (1×10^5/mouse) and intravenously (i.v.) injected with pelareorep (Pela; 2×10^8 plaque-forming units (pfu)/injection) on indicated days. Mice were sacrificed after 1, 2, or 3 Pela infusions for intratumoral analysis. **B,** Intratumoral presence of genomic copies of Reo S4 segment, as measured by qRT-PCR. **C,** Heat map depicting relative expression of various IFN response genes in tumors harvested after 1, 2, or 3 Pela infusions, as determined by qRT-PCR. **D,** Intratumoral frequency of NK cells within $CD45^+$ immune cells. **E,** Intratumoral frequency of $CD3^+$, $CD4^+$, and $CD8^+$ T cells within $CD45^+$ immune cells. **F,** Overview of experiment described in (**G** and **H**). Male C57BL/6J mice (n = 8–10/group) were subcutaneously inoculated with KPC3.TRP1 cells (1×10^5/mouse) and received intravenous injections with Pela (2×10^8 pfu/injection) and intraperitoneal (i.p.) injections with CD3xTRP1-bsAbs (12.5 µg/injection) on indicated days. **G,** Individual tumor growth curves of mice receiving indicated treatments. **H,** Kaplan–Meier survival graphs of mice after indicated treatments. Differences between groups in (**B, D,** and **E**) against the PBS-treated group was determined using an ordinary one-way ANOVA with the Dunnett's *post hoc* test. Log-rank tests were used to compare differences in survival in (**H**). Data represent mean±SEM. *, $P < 0.05$; **, $P < 0.01$; ****, $P < 0.0001$; ns, not significant. (**A** and **F,** Created with BioRender.com.)

monotherapy. However, our data strongly suggest that these efforts might not be necessary when Reo is used as an immunostimulatory agent. We expect that combined Reo and checkpoint blockade, which has already demonstrated potent responses in various preclinical models (57, 58) and is currently the subject of various clinical trials, as well as other combinatorial strategies that rely on effective Reo-induced influx of T cells, such as T-cell engagers (3), vaccination (33) or the use of dual-specific CAR T cells (59), should have potent antitumor responses in the presence of NAbs. Thus, our data are encouraging for ongoing and future clinical trials investigating the efficacy of Reo and T cell–based immunotherapeutic strategies, even in the context of intravenous Reo administration.

Altogether, given the high prevalence of seropositivity for Reo in patients with cancer, this study strongly advocates for the use of Reo as part of T cell–based combinatorial approaches if we are to unleash its full potential and allow maximal anticancer efficacy, without obstruction by preexisting immune responses.

Authors' Disclosures

M. Coffey reports personal fees from Oncolytics Biotech Inc. during the conduct of the study and personal fees from Oncolytics Biotech Inc. outside the submitted work, as well as reports 133 issued or pending patents related to reovirus, and with royalties paid from Oncolytics Biotech Inc. H. Loghmani reports personal fees from Oncolytics Biotech outside the submitted work and employment with Oncolytics Biotech, which owns pelareorep. T. van Hall reports grants from Oncolytics Biotech Inc. and Support Casper during the conduct of the study as well as grants from Genmab outside the submitted work. N. van Montfoort reports grants from Leiden University Medical Center, Stichting Overleven met Alvleesklierkanker (Dutch non-profit Foundation that supports pancreatic cancer research), and Oncolytics Biotech Inc. during the conduct of the study as well as grants from Dutch Cancer Society and Stichting Overleven met Alvleesklierkanker (Dutch nonprofit foundation that supports

pancreatic cancer research) outside the submitted work. No disclosures were reported by the other authors.

Authors' Contributions

C. Groeneveldt: Conceptualization, formal analysis, investigation, visualization, methodology, writing–original draft, writing–review and editing. **P. Kinderman:** Investigation, methodology. **L. Griffioen:** Methodology. **O. Rensing:** Investigation. **C. Labrie:** Methodology. **D.J.M. van den Wollenberg:** Resources, methodology. **R.C. Hoeben:** Resources, methodology. **M. Coffey:** Resources. **H. Loghmani:** Resources. **E.M.E. Verdegaal:** Resources. **M.J.P. Welters:** Resources. **S.H. van der Burg:** Writing–review and editing. **T. van Hall:** Conceptualization, funding acquisition, writing–review and editing. **N. van Montfoort:** Conceptualization, supervision, funding acquisition, writing–original draft, writing–review and editing.

Acknowledgments

The authors gratefully acknowledge John Hiscott and Michela Muscolini (Istituto Pasteur Italia-Fondazione Cenci Bolognetti, Rome, Italy) for the use of the VSVΔM51-GFP virus and Ajinkya Manelkar for practical assistance. The authors are also grateful to the operators of the Flow Cytometry Core Facility (FCF) of the LUMC and the Animal Facility of the LUMC for their excellent support and care of the animals, respectively. The hybridoma 10F6 (reovirus μ1), developed by T.S. Dermody from the University of Pittsburgh School of Medicine, was obtained from the Developmental Studies Hybridoma Bank, created by the NICHD of the NIH and maintained at the Department of Biology, The University of Iowa, Iowa City, IA. This work was financially supported by a fellowship from LUMC, a research grant from Oncolytics Biotech Inc. (to T. van Hall and N. van Montfoort) and the Support Casper campaign by the Dutch foundation "Stichting Overleven met Alvleesklierkanker" (supportcasper.nl) project number SOAK 22.02 (to N. van Montfoort).

Note

Supplementary data for this article are available at Cancer Immunology Research Online (http://cancerimmunolres.aacrjournals.org/).

Received June 8, 2023; revised October 31, 2023; accepted January 5, 2024; published first January 9, 2024.

References

1. Groeneveldt C, van Hall T, van der Burg SH, Ten Dijke P, van Montfoort N. Immunotherapeutic potential of TGFβ inhibition and oncolytic viruses. Trends Immunol 2020;41:406–20.
2. Müller L, Berkeley R, Barr T, Ilett E, Errington-Mais F. Past, present, and future of oncolytic reovirus. Cancers 2020;12:3219.
3. Groeneveldt C, Kinderman P, van den Wollenberg DJM, van den Oever RL, Middelburg J, Mustafa DAM, et al. Preconditioning of the tumor microenvironment with oncolytic reovirus converts CD3-bispecific antibody treatment into effective immunotherapy. J Immunother Cancer 2020;8:e001191.
4. Morris DG, Feng X, DiFrancesco LM, Fonseca K, Forsyth PA, Paterson AH, et al. REO-001: a phase I trial of percutaneous intralesional administration of reovirus type 3 dearing (Reolysin) in patients with advanced solid tumors. Invest New Drugs 2013;31:696–706.
5. Vidal L, Pandha HS, Yap TA, White CL, Twigger K, Vile RG, et al. A Phase I study of intravenous oncolytic reovirus Type 3 dearing in patients with advanced cancer. Clin Cancer Res 2008;14:7127–37.
6. Forsyth P, Roldán G, George D, Wallace C, Palmer CA, Morris D, et al. A Phase I trial of intratumoral administration of reovirus in patients with histologically confirmed recurrent malignant gliomas. Mol Ther 2008;16:627–32.
7. Groeneveldt C, van den Ende J, van Montfoort N. Preexisting immunity: barrier or bridge to effective oncolytic virus therapy? Cytokine Growth Factor Rev 2023; 70:1–12.
8. Tai JH, Williams JV, Edwards KM, Wright PF, Crowe JJE, Dermody TS. Prevalence of reovirus-specific antibodies in young children in Nashville, Tennessee. J Infect Disease 2005;191:1221–4.
9. White CL, Twigger KR, Vidal L, De Bono JS, Coffey M, Heinemann L, et al. Characterization of the adaptive and innate immune response to intravenous oncolytic reovirus (Dearing type 3) during a phase I clinical trial. Gene Ther 2008;15:911–20.
10. Lolkema MP, Arkenau H-T, Harrington K, Roxburgh P, Morrison R, Roulstone V, et al. A Phase I study of the combination of intravenous reovirus Type 3 dearing and gemcitabine in patients with advanced cancer. Clin Cancer Res 2011; 17:581–8.
11. Comins C, Spicer J, Protheroe A, Roulstone V, Twigger K, White CM, et al. REO-10: a Phase I study of intravenous reovirus and docetaxel in patients with advanced cancer. Clin Cancer Res 2010;16:5564–72.
12. Galanis E, Markovic SN, Suman VJ, Nuovo GJ, Vile RG, Kottke TJ, et al. Phase II trial of intravenous administration of Reolysin (Reovirus Serotype-3-dearing Strain) in patients with metastatic melanoma. Mol Ther 2012;20:1998–2003.
13. Adair RA, Roulstone V, Scott KJ, Morgan R, Nuovo GJ, Fuller M, et al. Cell carriage, delivery, and selective replication of an oncolytic virus in tumor in patients. Sci Transl Med 2012;4:138ra77.
14. Berkeley RA, Steele LP, Mulder AA, van den Wollenberg DJM, Kottke TJ, Thompson J, et al. Antibody-neutralized reovirus is effective in oncolytic virotherapy. Cancer Imm Res 2018;6:1161–73.
15. Ilett E, Kottke T, Donnelly O, Thompson J, Willmon C, Diaz R, et al. Cytokine conditioning enhances systemic delivery and therapy of an oncolytic virus. Mol Ther 2014;22:1851–63.
16. van den Wollenberg DJM, Dautzenberg IJC, van den Hengel SK, Cramer SJ, de Groot RJ, Hoeben RC. Isolation of reovirus T3D mutants capable of infecting human tumor cells independent of junction adhesion molecule-A. PLoS ONE 2012;7:e48064.
17. Smith RE, Zweerink HJ, Joklik WK. Polypeptide components of virions, top component, and cores of reovirus type 3. Virology 1969;39:791–810.
18. Fallaux FJ, Kranenburg O, Cramer SJ, Houweling A, Van Ormondt H, Hoeben RC, et al. Characterization of 911: a new helper cell line for the titration and propagation of early region 1–deleted adenoviral vectors. Hum Gene Ther 1996; 7:215–22.
19. Stojdl DF, Lichty BD, tenOever BR, Paterson JM, Power AT, Knowles S, et al. VSV strains with defects in their ability to shutdown innate immunity are potent systemic anti-cancer agents. Cancer Cell 2003;4:263–75.
20. Muscolini M, Hiscott J, Tassone EA. Genome-wide CRISPR-Cas9 loss-of-function screening to identify host restriction factors modulating oncolytic virotherapy. In: Krämer OH, editor. HDAC/HAT Function Assessment and Inhibitor Development: Methods and Protocols. New York, NY: Springer US; 2023. p. 379–99.
21. Dijkgraaf EM, Santegoets SJ, Reyners AK, Goedemans R, Wouters MC, Kenter GG, et al. A phase I trial combining carboplatin/doxorubicin with tocilizumab, an anti-IL-6R monoclonal antibody, and interferon-α2b in patients with recurrent epithelial ovarian cancer. Ann Oncol 2015;26:2141–9.
22. Verdegaal E, van der Kooij MK, Visser M, van der Minne C, de Bruin L, Meij P, et al. Low-dose interferon-alpha preconditioning and adoptive cell therapy in patients with metastatic melanoma refractory to standard (immune) therapies: a phase I/II study. J Immunother Cancer 2020;8:e000166.
23. Santegoets SJ, van Ham VJ, Ehsan I, Charoentong P, Duurland CL, van Unen V, et al. The anatomical location shapes the immune infiltrate in tumors of same etiology and affects survival. Clin Cancer Res 2019;25:240–52.
24. Speetjens FM, Kuppen PJ, Welters MJ, Essahsah F, Voet van den Brink AM, Lantrua MG, et al. Induction of p53-specific immunity by a p53 synthetic long peptide vaccine in patients treated for metastatic colorectal cancer. Clin Cancer Res 2009;15:1086–95.
25. Hingorani SR, Wang L, Multani AS, Combs C, Deramaudt TB, Hruban RH, et al. Trp53R172H and KrasG12D cooperate to promote chromosomal instability and widely metastatic pancreatic ductal adenocarcinoma in mice. Cancer Cell 2005;7: 469–83.
26. Benonisson H, Altıntaş I, Sluijter M, Verploegen S, Labrijn AF, Schuurhuis DH, et al. CD3-bispecific antibody therapy turns solid tumors into inflammatory sites but does not install protective memory. Mol Cancer Ther 2019;18:312–22.
27. Lin K-Y, Guarnieri FG, Staveley-O'Carroll KF, Levitsky HI, August JT, Pardoll DM, et al. Treatment of established tumors with a novel vaccine that enhances

major histocompatibility Class II presentation of tumor antigen. Cancer Res 1996;56:21–6.
28. Ruibal P, Franken K, van Meijgaarden KE, Walters LC, McMichael AJ, Gillespie GM, et al. Discovery of HLA-E–presented epitopes: MHC-E/peptide binding and T-cell recognition. Methods Mol Biol 2022;2574:15–30.
29. Belkina AC, Ciccolella CO, Anno R, Halpert R, Spidlen J, Snyder-Cappione JE. Automated optimized parameters for T-distributed stochastic neighbor embedding improve visualization and analysis of large datasets. Nat Commun 2019;10:5415.
30. Murphy JP, Kim Y, Clements DR, Konda P, Schuster H, Kowalewski DJ, et al. Therapy-induced MHC I ligands shape neo-antitumor CD8 T-cell responses during oncolytic virus-based cancer immunotherapy. J Proteome Res 2019;18:2666–75.
31. Mijatovic-Rustempasic S, Tam KI, Kerin TK, Lewis JM, Gautam R, Quaye O, et al. Sensitive and specific quantitative detection of rotavirus a by one-step real-time reverse transcription-PCR assay without antecedent double-stranded-RNA denaturation. J Clin Microbiol 2013;51:3047–54.
32. Dupont WD, Plummer WD Jr. Power and sample size calculations. A review and computer program. Control Clin Trials 1990;11:116–28.
33. Groeneveldt C, Kinderman P, van Stigt Thans JJC, Labrie C, Griffioen L, Sluijter M, et al. Preinduced reovirus-specific T-cell immunity enhances the anticancer efficacy of reovirus therapy. J Immunother Cancer 2022;10:e004464.
34. Loken SD, Norman K, Hirasawa K, Nodwell M, Lester WM, Demetrick DJ. Morbidity in immunosuppressed (SCID/NOD) mice treated with reovirus (Dearing 3) as an anti-cancer biotherapeutic. Cancer Biol Ther 2004;3:734–8.
35. Kim M, Garant KA, zur Nieden NI, Alain T, Loken SD, Urbanski SJ, et al. Attenuated reovirus displays oncolysis with reduced host toxicity. Br J Cancer 2011;104:290–9.
36. Dina Zita M, Phillips MB, Stuart JD, Kumarapeli AR, Snyder AJ, Paredes A, et al. The M2 gene is a determinant of reovirus-induced myocarditis. J Virol 2022;96:e0187921.
37. Samson A, Scott KJ, Taggart D, West EJ, Wilson E, Nuovo GJ, et al. Intravenous delivery of oncolytic reovirus to brain tumor patients immunologically primes for subsequent checkpoint blockade. Sci Transl Med 2018;10:eaam7577.
38. Collienne M, Loghmani H, Heineman TC, Arnold D. GOBLET: a Phase I/II study of pelareorep and atezolizumab ± chemo in advanced or metastatic gastrointestinal cancers. Future Oncol 2022;18:2871–8.
39. Sivanandam V, LaRocca CJ, Chen NG, Fong Y, Warner SG. Oncolytic viruses and immune checkpoint inhibition: the best of both worlds. Mol Ther Oncolytics 2019;13:93–106.
40. Kleinovink JW, Marijt KA, Schoonderwoerd MJA, van Hall T, Ossendorp F, Fransen MF. PD-L1 expression on malignant cells is no prerequisite for checkpoint therapy. Oncoimmunology 2017;6:e1294299.
41. Manso L, Salvador F, Villagrasa P, Chic N, Bermejo B, Cejalvo JM, et al. Abstract CT191: a window-of-opportunity study with atezolizumab and the oncolytic virus pelareorep in early breast cancer (AWARE-1). Cancer Res 2021;81:CT191–CT.
42. Arnold D, Collienne M, Stein A, Ungerechts G, Goekkurt E, Chater J, et al. 650 Pelareorep combined with atezolizumab and chemotherapy demonstrates encouraging results as first-line treatment in advanced or metastatic pancreatic ductal adenocarcinoma (PDAC) patients—interim results from the GOBLET study. J Immunother Cancer 2022;10:A681–A.
43. Ricca JM, Oseledchyk A, Walther T, Liu C, Mangarin L, Merghoub T, et al. Pre-existing immunity to oncolytic virus potentiates its immunotherapeutic efficacy. Mol Ther 2018;26:1008–19.
44. Tokunaga R, Zhang W, Naseem M, Puccini A, Berger MD, Soni S, et al. CXCL9, CXCL10, CXCL11/CXCR3 axis for immune activation—a target for novel cancer therapy. Cancer Treat Rev 2018;63:40–7.
45. Vitiello GAF, Ferreira WAS, Cordeiro de Lima VC, Medina TDS. Antiviral responses in cancer: boosting antitumor immunity through activation of interferon pathway in the tumor microenvironment. Front Immunol 2021;12:782852.
46. Geoffroy K, Bourgeois-Daigneault M-C. The pros and cons of interferons for oncolytic virotherapy. Cytokine Growth Factor Rev 2020;56:49–58.
47. van Montfoort N, Mangsbo SM, Camps MGM, van Maren WWC, Verhaart IEC, Waisman A, et al. Circulating specific antibodies enhance systemic cross-priming by delivery of complexed antigen to dendritic cells *in vivo*. Eur J Immunol 2012;42:598–606.
48. Ilett EJ, Bárcena M, Errington-Mais F, Griffin S, Harrington KJ, Pandha HS, et al. Internalization of oncolytic reovirus by human dendritic cell carriers protects the virus from neutralization. Clin Cancer Res 2011;17:2767–76.
49. Roulstone V, Khan K, Pandha HS, Rudman S, Coffey M, Gill GM, et al. Phase I trial of cyclophosphamide as an immune modulator for optimizing oncolytic reovirus delivery to solid tumors. Clin Cancer Res 2015;21:1305–12.
50. Ghiringhelli F, Menard C, Puig PE, Ladoire S, Roux S, Martin F, et al. Metronomic cyclophosphamide regimen selectively depletes $CD4^{+}CD25^{+}$ regulatory T cells and restores T and NK effector functions in end stage cancer patients. Cancer Immunol Immunother 2007;56:641–8.
51. Scurr M, Pembroke T, Bloom A, Roberts D, Thomson A, Smart K, et al. Low-dose cyclophosphamide induces antitumor T-cell responses, which associate with survival in metastatic colorectal cancer. Clin Cancer Res 2017;23:6771–80.
52. Qiao J, Wang H, Kottke T, White C, Twigger K, Diaz RM, et al. Cyclophosphamide facilitates antitumor efficacy against subcutaneous tumors following intravenous delivery of reovirus. Clin Cancer Res 2008;14:259–69.
53. Kottke T, Thompson J, Diaz RM, Pulido J, Willmon C, Coffey M, et al. Improved systemic delivery of oncolytic reovirus to established tumors using preconditioning with cyclophosphamide-mediated treg modulation and interleukin-2. Clin Cancer Res 2009;15:561–9.
54. Roulstone V, Mansfield D, Harris RJ, Twigger K, White C, de Bono J, et al. Antiviral antibody responses to systemic administration of an oncolytic RNA virus: the impact of standard concomitant anticancer chemotherapies. J Immunother Cancer 2021;9:e002673.
55. Weinstein R. Basic principles of therapeutic plasma exchange. Transfus Apher Sci 2023;62:103675.
56. Braun N, Bosch T. Immunoadsorption, current status, and future developments. Expert Opin Investig Drugs 2000;9:2017–38.
57. Mostafa AA, Meyers DE, Thirukkumaran CM, Liu PJ, Gratton K, Spurrell J, et al. Oncolytic reovirus and immune checkpoint inhibition as a novel immunotherapeutic strategy for breast cancer. Cancers 2018;10:205.
58. Augustine T, John P, Friedman T, Jiffry J, Guzik H, Mannan R, et al. Potentiating effect of reovirus on immune checkpoint inhibition in microsatellite stable colorectal cancer. Front Oncol 2022;12:1018767.
59. Evgin L, Kottke T, Tonne J, Thompson J, Huff AL, van Vloten J, et al. Oncolytic virus-mediated expansion of dual-specific CAR T cells improves efficacy against solid tumors in mice. Sci Transl Med 2022;14:eabn2231.